J. exp. Biol. ***185****, 207–249 (1993)*
Printed in Great Britain © The Company of Biologists Limited 1993

DYNAMIC MECHANICAL PROPERTIES OF PASSIVE SINGLE CARDIAC FIBERS FROM THE CRAB *CANCER MAGISTER*

EDGAR MEYHÖFER*

Department of Zoology, NJ-15, University of Washington, Seattle, WA 98195, USA

Accepted 11 August 1993

Summary

I determined the dynamic mechanical properties of single relaxed cardiac fibers from the Dungeness crab *Cancer magister*. Single fibers were mechanically isolated, chemically skinned and subjected to small-amplitude sinusoidal length perturbations over a wide range of strain rates and sarcomere lengths to characterize their viscoelastic behavior. The observed mechanical properties, together with transcardiac pressure recordings and ultrastructural measurements, were related to the overall function of the heart.

Single fibers, often longer than 1mm, could be mechanically dissected from the heart of *Cancer magister*. They typically ranged from 20 to 100 μm in diameter and were surrounded by a 100–400nm thick extracellular matrix. *In situ*, under normal physiological loads, the heart of *Cancer magister* generated transcardiac pressures of about 1000Pa and beat at 1Hz, while the sarcomere lengths of fibers changed by 10% from about 4.0 to 4.4 μm during contractions. The total stiffness of all fibers increased from approximately 0.01MPa to 1MPa in the sarcomere length range from 3.8 to 6.0 μm and increased two- to threefold with a rise in strain rate from 0.01 to 5rad s^{-1}. In the physiological range of sarcomere length (4.0–4.4 μm) and strain rate (0.5–1.2rad s^{-1}), single cardiac fibers behaved viscoelastically, with average values for the relative energy dissipation ranging from 0.5 to 0.7. The volume fraction of the extracellular matrix correlated positively with the stiffness of single cardiac fibers.

On the basis of these results, I propose a dual role for the viscoelastic behavior of *Cancer magister* cardiac fibers: (1) the viscous energy dissipation confers dynamic mechanical stability at the level of the single fiber, and (2) the storage and return of elastic strain energy saves energy at the level of the whole heart.

Introduction

The passive mechanical behavior of cardiac and skeletal muscle is commonly viewed as dominantly elastic, with any viscous component contributing little to the muscle's overall mechanical behavior (see Hoyle, 1983; Gordon, 1989). It is widely believed that

*Present address: Department of Physiology and Biophysics, SJ-40, University of Washington, Seattle WA 98195, USA.

Key words: muscle, heart, mechanics, ultrastructure, energetics, viscoelasticity, extracellular matrix, *Cancer magister*.

the functional role of this mechanical behavior is to prevent overextension of the fibers. The importance of this function has been emphasized in vertebrate cardiac muscle, which is considerably stiffer than skeletal muscle (Strobeck and Sonnenblick, 1989).

Meyhöfer and Daniel (1990) have recently measured the dynamic mechanical properties of extensor fibers from the shrimp *Pandalus danae*. These fibers are rapidly loaded during the shrimp's escape maneuver. The extensor fibers are characterized by a large viscous component in their mechanical behavior. Although the implications of such high viscous damping are not clear, Meyhöfer and Daniel (1990) suggested that such damping may provide dynamic stability to rapidly deformed cells.

A challenge to the dynamic stability hypothesis comes from mechanical data from muscle fibers that experience slow and continuous deformations. One might argue that the rapid nature of the escape response and the discontinuous mode of operation of the extensor fibers represent a very specialized mechanical environment that requires a unique mechanism, namely viscous damping, to maintain mechanical stability. However, a few authors have reported some form of viscoelastic behavior in other passive muscles. For example, Pinto and Fung (1973) measured the stress relaxation behavior of rabbit papillary muscle, and Buchthal and Rosenfalck (1957) demonstrated hysteresis during sinusoidal oscillation of isolated frog fibers. In order to test whether the observation of viscoelastic mechanical behavior is applicable to a wider variety of muscle, I investigated the dynamic mechanical properties of a slowly and continuously operating muscle system: crustacean cardiac fibers.

Cardiac muscle is an ideal system with which to address this challenge. Hearts beat continuously and relatively slowly, and the physiologically relevant loading regime of cardiac fibers can be determined. However, single vertebrate cardiac fibers are small and are usually obtained through enzymatic cell isolation procedures. Unfortunately, enzymatic digestion destroys the extracellular matrix, which is believed to be a major determinant of the mechanical behavior of passive muscle fibers (Ramsey and Street, 1940; Tidball, 1986; Sonnenblick and Skelton, 1974). I overcame this difficulty by developing a single-fiber preparation from the heart of the Dungeness crab *Cancer magister*. Individual fibers, often longer than 1000 μm, can be obtained by mechanical dissection.

The main purpose of this paper is to describe the dynamic mechanical properties of single cardiac fibers over a wide range of sarcomere lengths and strain rates, including those that are physiologically relevant. Using such data, I address the following questions. (1) Is the cardiac muscle system characterized by viscoelastic behavior? (2) Is there significant viscous energy dissipation in the physiologically relevant range of sarcomere lengths and strain rates? (3) How do the mechanical properties of the single fibers relate to the overall function of the system?

Materials and methods

Animals

All experiments were carried out on single fibers isolated from hearts of the Dungeness crab *Cancer magister*. Healthy animals were obtained from a local vendor and held in a

large tank connected to the recirculating seawater system of the Department of Zoology, University of Washington, Seattle. The temperature was maintained between 12 and 13˚C. Animals that were kept longer than 2–3 days were regularly fed a diet of mussels or clams.

Pressure measurements

To determine the range of physiologically relevant frequencies and strain rates, transcardiac pressure recordings were made with a pressure transducer (Statham) connected to PE-40 Tygon tubing. The pressure transducer and tubing were filled with Millipore-filtered sea water. This apparatus had a frequency response well in excess of 20Hz. A hole, located directly over the heart, was drilled into the dorsal carapace of a crab using a small dentist's drill. The bevelled end of the Tygon tubing was inserted into the heart and secured with dental wax. The crab was returned to a small seawater aquarium (0.5 m×0.5 m×0.15m deep, 12–13˚C) and allowed to move around freely. Crabs recovered quickly from this procedure and began ventilating normally within a very short time. All crabs studied survived this procedure without any complications.

Pressure transducer signals were conditioned using a standard Wheatstone bridge amplifier and collected with a data acquisition system (described below) at 200Hz sampling frequency. Several records each containing 16383 data points (record length greater than 80s) were saved on floppy disk for later analysis. The pressure transducer, calibrated with known heads of water, had a sensitivity of 596.3Pa V^{-1}.

Cell isolation

Crabs were killed by rapidly destroying the brain with a large pair of bone rongeurs. The dorsal aspect of the carapace was carefully removed. The heart was excised and immersed in a large Sylgard dish (Sylgard 184 Elastomer, Dow Corning) containing cooled calcium-free crustacean Ringer (for details of all solutions, see the next paragraph). At this point, the heart was usually still beating, because the blood inside the heart had not been exchanged completely for calcium-free Ringer. The heart, pinned down at its lateral margins and the dorsal side, containing the four ostia, was carefully cut open with small scissors. This procedure exposed two relatively small groups of fibers running in the anterior–posterior direction. These groups of fibers were then removed and placed in a Sylgard-lined dish containing a cooled skinning solution with 0.5% of the detergent Chaps {3-[(3-cholamidpropyl)-dimethylammonio]-1-propanesulfonate, Sigma} to solubilize the cell membranes. After 30s, the skinning solution was washed out with several changes of relaxing solution (see below) to ensure complete removal of the detergent. The groups of fibers were pinned down with fine stainless-steel minuten pins (0.1mm diameter, Fine Science Tools) and placed on a cooled black aluminum stage under a high-power dissecting microscope (Zeiss). Single fibers were dissected from these bundles using Dumont no. 5 forceps with extra-fine tips and a pair of ultrafine Vannas spring scissors. Fibers longer than 1000 μm could be dissected routinely from these bundles, and it was not uncommon to obtain fibers longer than 2000 μm. Fibers showing any signs of mechanical damage were rejected.

Solutions

The intracellular solutions used for experiments reported in this paper were prepared according to the methodology described by Fabiato and Fabiato (1979). Solutions for skinned fiber preparations (intracellular solutions) contained several ligands [EGTA (Sigma), ATP (Sigma), ADP (Sigma), phosphate and a buffer)], metals (Ca^{2+}, Mg^{2+}, K^{+}) and H^{+}. The steady-state concentration of each species in a complex mixture of these metals and ligands is described by the multiple equilibria between individual metals and ligands. In addition, the stability (or binding or association) constants describing individual metal and ligand interactions depend on temperature and ionic strength. Given the ionic strength, the pH and the free and/or total concentration of relevant metals and ligands, the total and free concentrations of each chemical species were calculated by solving the system of equations describing all equilibrium states. This calculation was carried out using a modified computer program generously provided by Dr A. M. Gordon (Department of Physiology and Biophysics, University of Washington, Seattle). The equilibrium constants were taken from various references summarized in the paper of Brozovich *et al.* (1988, Table 1). I used Mops (Sigma) as a buffer; its concentration was iteratively determined such that a total ionic strength of 200mmol l^{-1} and a pH of 7.0 was maintained in all solutions. The major anion was propionate. The exact composition of the three solutions is given in Table 1.

Experimental chamber

The experimental chamber was approximately 17mm long, 8mm wide and 4mm high. The sides were cut from 1mm thick microscope slides (2948, Corning) and assembled with silicone rubber (Dow Corning) in the middle of a 75mm by 50mm microscope slide. During experiments, this chamber was pressed firmly against the Peltier-cooled copper stage with a set of microscope slide clips to ensure proper cooling of the solution in the chamber. Temperature was monitored with a digital thermocouple thermometer (TH 65, Wescor).

Mechanical testing apparatus

The mechanical testing apparatus consisted of a length displacement generator and a force transducer between which the single fiber was mounted. From instantaneous measurements of the length perturbations of the fiber and the resulting forces, all the required mechanical properties could be calculated. Sinusoidal deformations were used throughout all experiments reported here. The length displacement driver and force

Table 1. *Solutions used in the experiments*

	Concentrations (mmol l^{-1})								
Solution	Total Na^{+}	Total K^{+}	Free Mg^{2+}	Free Ca^{2+}	Total EGTA	Total ATP	Total MOPS	Chaps	pH
Ca^{2+}-free Ringer	440	10	26	$<10^{-5}$	5		10		7.4
Skinning		130	3.16	10^{-6}	20	4.15	46.2	0.5%	7.0
Relaxing		130	3.16	10^{-6}	20	4.15	46.2		7.0

transducer were each mounted on *x*,*y*,*z*-micromanipulators (460-XYZ, Newport), attached to the stage of a large industrial microscope (UM-3, Nikon). The microscope stage (modified from a Nikon industrial microscope stage, type 2×402) was equipped with two Mitutoyo stage micrometer heads (series 152) that allowed movement of the stage in the *x*- and *y*-directions with 1 μm precision. In addition, the central portion of the stage could be move in the *z*-direction and had a thermally isolated copper plate that was cooled by a Peltier (FC-06-66-05L, Melcor) element.

Force transducer and bridge amplifier

The force transducer was made from a small piece of brass 0.05mm thick, 9mm wide and 6mm long. A pair of fine stainless-steel needles was silver-soldered to the end of this beam. The needles were ground flat and carefully demagnetized. A pair of semiconductor strain gauges (Micro Engineering II) was mounted on each side of the beam using an epoxy adhesive (M-Bond 610, Micro-Measurements). These four gauges formed a Wheatstone bridge that was powered with 4mA of current and the output of which was amplified with a precision instrumentation amplifier (AD 624, Analog Devices). The major sources of error degrading the performance of the force transducer are thermal shifts in the gauge factor and the resistance of individual strain gauges. To minimize these thermal errors, the bridge amplifier was equipped with a passive resistor network.

The force transducer was calibrated by suspending small weights made from aluminum foil from the tips of the horizontally mounted transducer and recording the resultant signals. The force transducer used for the experiments described in this paper had a sensitivity of $121.96\,\mathrm{V\,mN^{-1}}$ and behaved extremely linearly over the range of forces measured here, as indicated by the good fit to a linear regression model (r^2=0.9997, N=60). The displacement sensitivity of the transducer was measured by displacing its tip dynamically with the piezoelectric length driver (see below). This force transducer had a displacement sensitivity of $0.602\,\mathrm{V\,\mu m^{-1}}$. Again, this relationship was extremely linear (r^2=0.9998, N=80). Using both calibration results, the compliance of the transducer was calculated to be $0.202\,\mathrm{m\,N^{-1}}$. The resonance frequency of the transducer was 150Hz. Test samples of small pieces of rubber and steel wire showed no measurable phase lag between displacement and force signals at all frequencies below 150Hz. At 150Hz, however, significant ringing was noted in the force transducer.

Length displacement driver and sensor

The length driver was a piezoelectric bimorph to which a pair of needles identical to those on the force transducer was mounted. The deformation of the bimorph was controlled by the voltage applied to the crystal. Since the exact displacement of a piezoelectric bimorph changes with both load and frequency, the actual movement of the driver must be tracked. This was done using an electro-optical method with very high spatial and temporal accuracy. The position of the needle pair on the length driver, imaged with a long working distance objective (Nikon M Plan 40, 0.5 NA), was projected onto a diffuse silicon detector (Spot 2D, United Detector Technology). The detector consisted of two individual photodiodes, 1.25mm×2.5mm in size, separated by a very small gap (approximately 0.1mm). The detector was positioned in the phototube so that

the image of the needle was projected onto the light-sensitive surface in the same direction as the gap between the two diodes and covered approximately equal areas of both diodes. The image magnification was chosen such that half of each photodiode was covered. The ouputs of the diodes were monitored with standard transimpedance amplifiers (OPA 111 BM, Burr Brown). The difference between the signals from the two diodes was linearly proportional to the displacement of the needle (given constant illumination) and, owing to the high common-mode rejection of the differential amplifier (INA 101 BM, Burr Brown), contained little noise. The halogen light source of the microscope was operated with a stabilized d.c. power supply to avoid the intensity fluctuations associated with standard a.c. operation. In addition, an analog circuit (DIV 100, Burr Brown) was built to divide the difference between the outputs by their sum. This procedure made the displacement signal independent of the intensity of illumination. The optical sensor had a frequency response better than 10kHz. Calibration was accomplished with a filar micrometer. The sensitivity of the displacement sensor was $103.3\,\mathrm{mV}\,\mu\mathrm{m}^{-1}$ and was linear over the measurement range from 0 to $50\,\mu\mathrm{m}$ (r^2=0.99998, N=9).

Computer control and acquisition system

Sinusoidal length changes and data acquisition were both under computer control. The analog output port of the data acquisition board (DT 2801, Data Translations) was programmed to drive a voltage-to-frequency converter (XR-2206, Exar). In this way, both the amplitude and the frequency of the sine wave were under computer control. The output of the voltage-to-frequency converter was fed into a high-voltage power buffer (Underware Electronics) that controlled the piezoelectric length driver.

Instantaneous force and displacement signals were collected with the analog input port of the data acquisition board. Either 1024 or 2048 points of each signal were sampled. The acquisition rate was set to sample exactly an integer number of sine waves (at least 16). A typical experimental run proceeded as follows: (1) amplitude and frequency of the sine wave were set; (2) the single fiber was oscillated for an integer number of sine waves at that particular frequency and amplitude, and instantaneous voltages corresponding to force and displacement were digitized and stored in RAM; (3) these two steps were repeated for 20 or 25 frequencies ranging from below 0.1Hz to about 50Hz. At the end of the last experiment, all data and control variables were stored on floppy disk for later processing.

An eight-pole two-channel low-pass Bessel filter limited the bandwidth of the force and displacement signal to reduce noise and to prevent aliasing. The filter was built with highly stable universal filters (UAF 41, Burr Brown) and low temperature coefficient resistors (Caddock Electronics). This device had identical transfer functions for both channels. Thus, no difference could be detected in the phase shift between the two channels.

Sarcomere length

Sarcomere length was determined by standard laser diffractometry (Squire, 1981). After a fiber had been loaded into the apparatus, the beam of a He–Ne laser was passed

through the center of the fiber. The laser was mounted on a *y,z*-micropositioner (430, Newport) with ultrafine micrometer screws to adjust the position of the beam in the fiber precisely. The distance between the primary diffraction lines was measured opto-electronically. Refraction of the diffraction lines at the solution–glass and glass–air interfaces was taken into account (Squire, 1981).

Opto-electronic measurement of the distance between the diffraction primaries was based on a photodetector (Spot 2D, United Detector Technology) similar in design to the one employed for position-sensing of the length driver. The sensor was mounted on a single-axis translating stage (430, Newport), equipped with a Vernier micrometer, and moved laterally until the relative position of the centroids had been determined. The distance between the primary diffraction lines was then simply the difference between the two relative centroid positions. This method was extremely precise; with good diffraction patterns, differences of 0.01 μm in sarcomere length could be detected.

Experimental protocol

Single fibers were isolated as described above and loaded into the mechanical testing apparatus. Throughout mechanical testing, fibers were kept in relaxing solution at 12–13°C. Uniformity of sarcomere length in fibers was evaluated by moving the laser beam laterally and measuring sarcomere length at several locations along the length of the fiber. If non-uniformities exceeded 0.2 μm, the fiber was rejected. In addition, the quality of fibers was evaluated under 100× magnification (10× CF Plan lens, NA 0.30, Nikon and 10× oculars, CFW, Nikon) using the measurement microscope and brightfield illumination. Any irregularities in the striation pattern or apparent injuries led to the rejection of the fiber.

Fibers of satisfactory quality were put under light tension by increasing their length slightly. Fiber length was determined by moving the mounted fiber under 100× magnification using the stage micrometer heads. This method allowed estimation of the fiber length (the length between the two microclamps) to approximately 1 μm. Fibers were then tested dynamically and the data were stored for later processing. This procedure was repeated at several different sarcomere lengths for each cell: fiber length was increased and the new fiber length and sarcomere length were measured.

Electron microscopy and extracellular matrix volume fraction

At the end of the experiments, fibers were fixed for electron and light microscopy. This allowed me (1) to verify independently the sarcomere length estimates from laser diffractometry, (2) to determine the potential physiological range of sarcomere length from the lengths of myofilaments, and (3) to determine the cell cross-sectional area, perimeter and volume fraction of extracellular matrix. Fiber length and cross-sectional area entered directly into the calculation of mechanical properties; hence, direct measurement of the irregular cross-sectional area from sections was necessary to reduce the variability of mechanical data between individual fibers.

Fibers were fixed by immersion in a solution of 5% glutaraldehyde (EM grade, Ted Pella) in 0.1mol l^{-1} sodium cacodylate (Ted Pella). The pH of the solution was adjusted

to 7.0. The fibers remained immersed in fixative for at least 20min while clamped in the apparatus before they were removed and transferred into a fresh volume of fixative. Fibers were stored in fixative at 5˚C until further processing.

In addition, a few pieces of cardiac tissue from intact fiber bundles were fixed for morphological and ultrastructural observations. One of the following fixatives was used: (1) 3% glutaraldehyde in $0.1\,mol\,l^{-1}$ sodium cacodylate with 18% sucrose (Baker); (2) 3% glutaraldehyde and 1.5% paraformaldehyde (Polysciences) in $0.1\,mol\,l^{-1}$ sodium cacodylate with 18% sucrose, $5\,mmol\,l^{-1}$ EGTA and $4\,mmol\,l^{-1}$ magnesium chloride; (3) 4% glutaraldehyde in $0.2\,mmol\,l^{-1}$ sodium cacodylate buffer. Included in this last fixative were $0.4\,mol\,l^{-1}$ sucrose, $0.1\,mmol\,l^{-1}$ sodium chloride, $3\,mmol\,l^{-1}$ EGTA and $3\,mmol\,l^{-1}$ magnesium chloride. The pH of all fixatives was adjusted to 7.4. Fixative was perfused into the heart by direct injection. All fixatives were about equally successful in preserving the contractile apparatus of these cardiac fibers, but preservation of the cytoplasmic ground substance proved very difficult. The third fixative produced moderately better results in preserving the fine structure of the cytoplasm.

Primary fixative was carefully washed out in $0.1\,mol\,l^{-1}$ sodium cacodylate buffer and fibers were then postfixed for 1h in 1% osmium tetroxide, buffered in $0.1\,mol\,l^{-1}$ sodium cacodylate. The postfixative was washed out with $0.1\,mol\,l^{-1}$ sodium cacodylate buffer and distilled water, and the fibres were then rapidly dehydrated in a graded series of ethanols. Fibers were infiltrated with a standard mixture of Epon (Polybed 812, Polysciences) using propylene oxide (analytical grade, Baker) as intermedium. Each fiber was bisected lengthwise. One piece was oriented in the embedding mold such that a cross section could be obtained, while the other was oriented for longitudinal sectioning.

The cross-sectional area and perimeter of each fiber were determined by preparing a $0.5\,\mu m$ cross section and digitizing *camera lucida* tracings of these sections. Tracing were prepared with a 100× oil-immersion objective (Nikon, 1.3 NA) and the highest magnification setting on the *camera lucida* (Nikon).

Since the extracellular matrix (ECM) measures only between 100 and 400nm in these fibers, its thickness had to be estimated by transmission electron microscopy (TEM). From each fiber, thin sections were cut in both the longitudinal and cross-sectional directions using a diamond knife (Diatome). Longitudinal sections were cut perpendicular to the long axis of the fiber to avoid compression. For cross sections, care was taken that the whole cross section was included. In each direction, five grids, each containing between 5 and 10 sections, were prepared. Sections were stained with uranyl acetate and lead citrate in the usual manner and viewed with a Philips 300 TEM. Quantitative measurements were made from a series of negatives documenting the morphology of the ECM at 50–100 μm intervals. About 25–50 measurements were taken from each cell. Negatives had an image magnification in the range from 5000 to 10000 times. Negatives of a calibrated replica grating (Ted Pella) at the same magnifications were included. The actual thickness of the ECM was measured directly from the negatives with the aid of a calibrated ocular micrometer and a dissecting microscope.

The volume fraction of the matrix (V_{ECM}) is given by:

$$V_{ECM} = t_{mean} P/A\,, \tag{1}$$

where t_{mean} is the mean thickness of the matrix, P is the fiber perimeter or ECM length and A is the cross-sectional area of the fiber.

Longitudinal sections were also used to estimated the myofilament length. The length of actin and myosin filaments and the sarcomere length were measured, from a set of randomly taken electron micrographs, in the same manner as described above.

Data analysis

Calculation of signal amplitudes and phase

The viscoelastic behavior is described by a complex valued modulus. This quantity was calculated in the following way: the one-sided power spectral (often called autospectral) density function was estimated using the fast Fourier transform (FFT) method (Bendat and Piersol, 1986, 1980, Priestley, 1981):

$$G_{xx}(f_k) = [2/(N\Delta t)]|X(f_k)|^2 \qquad \{k = 0, 1,..., N/2\}, \tag{2}$$

where:

$$X(f_k) = \Delta t \sum_{n=0}^{N-1} x_{in} \exp(-j2\pi kn/N), \tag{3a}$$

$$f_k = k/N\Delta t \qquad \{k = 0, 1, 2,..., N-1\} \tag{3b}$$

and j is taken to be the complex number $\sqrt{-1}$, N is the total number of data points in the record of length T, Δt is the sampling interval and $X(f)$ is the finite Fourier transform of the time series x_{in} (displacement or force record). I used a modified Cooley–Tukey algorithm (Borland International) for implementing the FFT method. The force and displacement records were transformed together as one single complex data record (Bendat and Piersol, 1986) using a rectangular data window. In addition, estimation of the one-sided autospectral density function gives an estimate of the harmonic amplitudes. Because an integer number of sine waves was contained in each data record, all the power of the signal is contained in a single complex pair of Fourier coefficients at the relevant frequency, rejecting noise outside the narrow signal band (bandwidth $1/T$) centered at the frequency n_w/T (n_w denoted an integer number of waves in the record). This signal processing strategy successfully eliminated most of the thermal noise of the force transducer.

The noise spectral density of the transducer is approximately 500mV/√Hz at 0.1Hz and drops very steeply to 0.4mV/√Hz at 1.0Hz. However, since I collected 16 waves of data in the frequency range of 0.1Hz, the noise signal entering into the data band is estimated to be approximately 125mV. At a typical signal amplitude of 1V, this noise corresponds to less than 2.0% of the power of the signal. At only slightly higher frequencies, the signal-to-noise ratio improves dramatically, because the noise power spectral density drops off so sharply.

The displacement sensor noise and resolution were limited by the bit resolution of the data acquisition board. I estimated the noise autospectral density to be 1mV/√Hz at 0.1Hz. The noise drops to about half this value at 1.0Hz. Thus, the displacement noise spectral density is about 10nm/√Hz (unity gain of the differential amplifier stage).

The phase between the force and displacement signal is calculated from the cross-spectral density function:

$$G_{xy}(f_k) = [2/(N\Delta t)][X^*(f_k)Y(f_k)], \qquad \{k = 0, 1, 2,..., N/2\} \tag{4}$$

where $X(f)$ and $Y(f)$ are the finite Fourier transforms of the time history records of force and displacement. The quantity $X^*(f)$ is the complex conjugate of $X(f)$. Note that the cross-spectral density function is complex; it is often expressed as:

$$G_{xy}(f_k) = C_{xy}(f_k) - jQ_{xy}(f_k), \qquad \{k = 0, 1, 2,..., N/2\} \tag{5}$$

where $C_{xy}(f_k)$ is the one-sided coincident spectral density function and $Q_{xy}(f_k)$ is the one-sided quadrature spectral density function (Bendat and Piersol, 1986; Priestley, 1981). With these spectral density functions, the phase spectrum is estimated directly by:

$$\theta_{xy}(f_k) = \tan^{-1}[Q_{xy}(f_k)/C_{xy}(f_k)]. \tag{6}$$

Calculation of corrected stress, strain and phase

Since the force transducer undergoes small displacements, its motion and associated phase must be taken into account when computing amplitudes and phases. The corrected strain amplitude is given by:

$$|\epsilon(f_k)| = \{[A(f_k) - B(f_k)\cos\theta_{xy}(f_k)]^2 + [B(f_k)\sin\theta_{xy}(f_k)]^2\}^{1/2}/l_0, \tag{7}$$

where $A(f_k)$ is the amplitude of the displacement length driver, $B(f_k)$ is the amplitude of the force transducer displacement, $\theta_{xy}(f_k)$ is the phase shift between the displacement and force signals (as calculated from equation 6) and l_0 is the length of the fiber. The amplitudes $A(f_k)$ and $B(f_k)$ are calculated from the appropriate power spectral density functions and calibrations. The adjusted phase (δ), that is the phase shift between stress and strain, is given by:

$$\delta(f_k) = \theta_{xy}(f_k) - \tan^{-1}\{B(f_k)\sin\theta_{xy}(f_k)/[B(f_k)\cos\theta_{xy}(f_k) - A(f_k)]\}. \tag{8}$$

The stress amplitude, $\sigma(f_k)$, requires no correction and is calculated by:

$$\sigma(f_k) = F(f_k)/A, \tag{9}$$

where $F(f_k)$ is the amplitude of the force signal and A is the cross-sectional area of the fiber. $F(f_k)$ was calculated, with the appropriate calibrations, from the force power autospectral density function (see equation 2). For fiber lengths other than the one at which the fiber was fixed, the cross-sectional area was calculated using the optically measured length and assuming constant fiber volume.

Calculation of moduli

The total dynamic stiffness is defined as:

$$|E^*(f_k)| = |\sigma(f_k)| / |\epsilon(f_k)|, \tag{10}$$

and is a measure of the resistance to dynamic deformation (Wainwright *et al.* 1976; Fung, 1981, 1984; Ferry, 1980). This quantity is identical to the magnitude of the complex valued modulus E^* and, for brevity, is called the complex modulus. I will also refer to the

total stiffness as the complex modulus. With a known phase and the complex modulus, two additional moduli are defined:

$$E'(f_k) = |E^*(f_k)|\cos[\delta(f_k)] \tag{11a}$$

and

$$E''(f_k) = |E^*(f_k)|\sin[\delta(f_k)]\ . \tag{11b}$$

The elastic (storage) modulus, E', represents the component of the stress response of the fiber that is in phase with the strain. Thus, it measures the ability of the fiber to store and return mechanical strain energy. The viscous or loss modulus, E'', measures the out-of-phase component of the stress response and hence quantifies the extent to which the fiber dissipates mechanical strain energy. The complex modulus (not its absolute value) is therefore equal to:

$$E^*(f_k) = E'(f_k) + jE''(f_k). \tag{12}$$

There is one more useful expression to describe the viscoelastic behavior of muscle fibers:

$$\tan[\delta(f_k)] = E''(f_k)/E'(f_k). \tag{13}$$

This ratio of the viscous to the elastic modulus is equal to the tangent of the phase angle between stress and strain (Wainwright *et al.* 1976) and therefore measures the relative energy dissipation of a viscoelastic material.

Analysis of pressure signals

Pressure records were analyzed by calculating the power spectral density functions. Records were cut into seven data sets each containing 4096 points. Data sets overlapped by 50%. Data were tapered with a Hanning window to reduce side-lobe leakage and the finite Fourier transforms were calculated as described above. The smoothed autospectral density function was constructed by first adjusting the scale factor for the loss due to data windowing and then calculating the ensemble average of the autospectral density function (Bendat and Piersol, 1986; Press *et al.* 1989).

Fitting a model to the mechanical response function

In order to condense and summarize the mechanical response surface of a number of fibers, I fitted the data to the following functions:

$$|E^*(\dot{\epsilon},\mathrm{sl})| = \{[a + b(\mathrm{sl}_\Delta)^c]\,(1 + d[1 - \exp(-e\dot{\epsilon})]\} \tag{14}$$

and

$$\tan[\delta(\dot{\epsilon},\mathrm{sl})] = f + [(g\dot{\epsilon})/(1 + h\dot{\epsilon}^2 + k\dot{\epsilon}\,\mathrm{sl}_\Delta + l\mathrm{sl}_\Delta^2)] \tag{15}$$

where $\dot{\epsilon}$ and sl_Δ are defined as:

$$\dot{\epsilon} = |d\epsilon/dt| = 2\pi f_r \epsilon \tag{16}$$

and

$$\mathrm{sl}_\Delta = 100[(\mathrm{sl} - 3.7)\ /\ 3.7]. \tag{17}$$

Here a, b, c, d, e, f, g, h, k and l are the variables of the model that need to be determined. The variable f_r stands for the frequency of oscillation. A model for both the total stiffness

$|E^*(\epsilon,sl)|$ and the relative energy dissipation, $\tan\delta(\epsilon,sl)$, was chosen to represent the viscoelastic behavior of the mechanical response surface. The independent variables in both models are strain rate ($\dot{\epsilon}$) and the relative sarcomere length extension (sl_Δ) (as a percentage) normalized to the low end of the physiological range of sarcomere length (for cardiac fibers: 3.7 μm).

The actual fitting (optimization of the parameters) of these nonlinear models was accomplished with a Levenberg–Marquardt algorithm (Press *et al*. 1989). I used the least-squares criterion as the figure-of-merit function. To evaluate whether the appropriate stopping conditions and the global minimum had been found, the least-squares minimization of the model was repeated with a wide variety of reasonable starting estimates for the variables. Consistently, all iterations 'walked' to the same minimum. The goodness of fit of the model was determined with *F*-test statistics (Bevington, 1969; Seber and Wild, 1989) assuming that the errors are independent and that they have zero mean, consistent variance and follow a normal distribution. Multiple regression equations were compared as outlined by Zar (1984).

Results

Morphology and ultrastructure of single cardiac fibers

Single cardiac fibers from large crabs typically range from 20 to 100 μm in diameter (Fig. 1). They contain numerous myofibrils that resemble those of skeletal muscle: each myofibril is about 2–4 μm wide and is characterized by a regular striation pattern. No intercalated discs were found (Fig. 1) in these or in any other sections. However, in contrast to skeletal muscle, these cardiac fibers have a large cytoplasmic volume fraction (Fig. 1A,B) and are often connected by cytoplasmic bridges. Also, individual fibers are not densely packed, but are separated in the intact heart. They often have highly irregular cross sections whose areas typically range from 1500 to 8400 μm^2 (see also Table 3).

The ultrastructural organization of cardiac myofibrils is fairly standard with I-bands, A-bands, Z- and M-lines and H-zones forming the characteristic striation pattern of the sarcomere (Fig. 1C). Myosin filaments in this preparation were about 3 μm long, whereas

Fig. 1. Morphology of intact cardiac muscle from *Cancer magister*. All micrographs shown in this figure were obtained from tissue fixed by direct injection of fixative into the heart. All sections were obtained from the same bundle of fibers that was used in the mechanical experiments. Sections for light microscopy were stained with Toluidine Blue. (A) High-magnification light micrograph of part of a single cardiac fiber. Individual myofibrils (*m*), about 2–4 μm wide, with the typical striation pattern are clearly visible. The cytoplasm (*c*) contains numerous mitochondria and nuclei (*nu*). Scale bar, 20 μm. (B) Longitudinal section through the fiber bundle from which single fibers for mechanical experiments were dissected. Individual fibers are separated by about 50 μm. The cytoplasm forms a wavy pattern on the fiber surface. Scale bar, 60 μm. (C) Low-magnification electron micrograph of several sarcomeres. The A-bands with the myosin filaments (*my*), I-band (I), H-band and Z-lines (*Z*) are clearly visible and give individual myofibrils their characteristic pattern of repeating sarcomeres. In addition, the band containing actin filaments (*ac*) can be discerned and the M-lines (*M*) are well defined. Mitochondria (*mi*) are located between individual myofibrils. Scale bar, 2 μm.

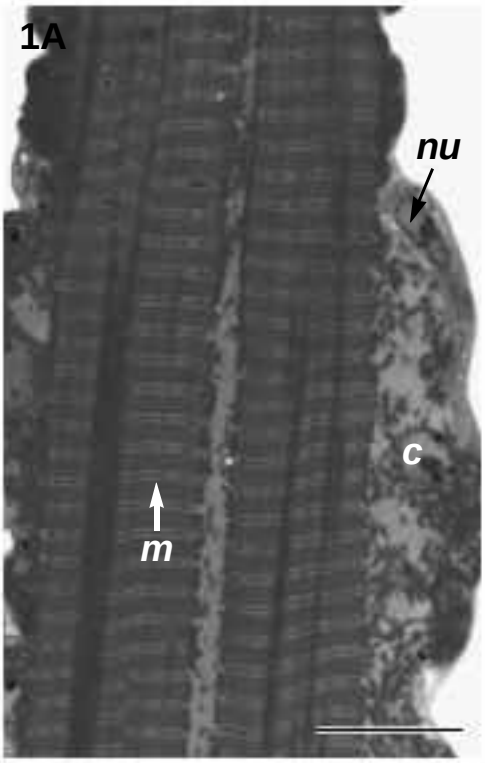
1A
nu
c
m

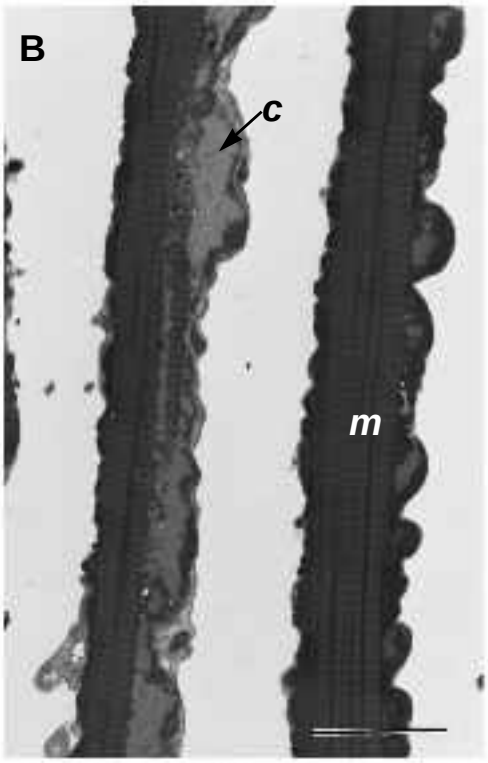
B
c
m

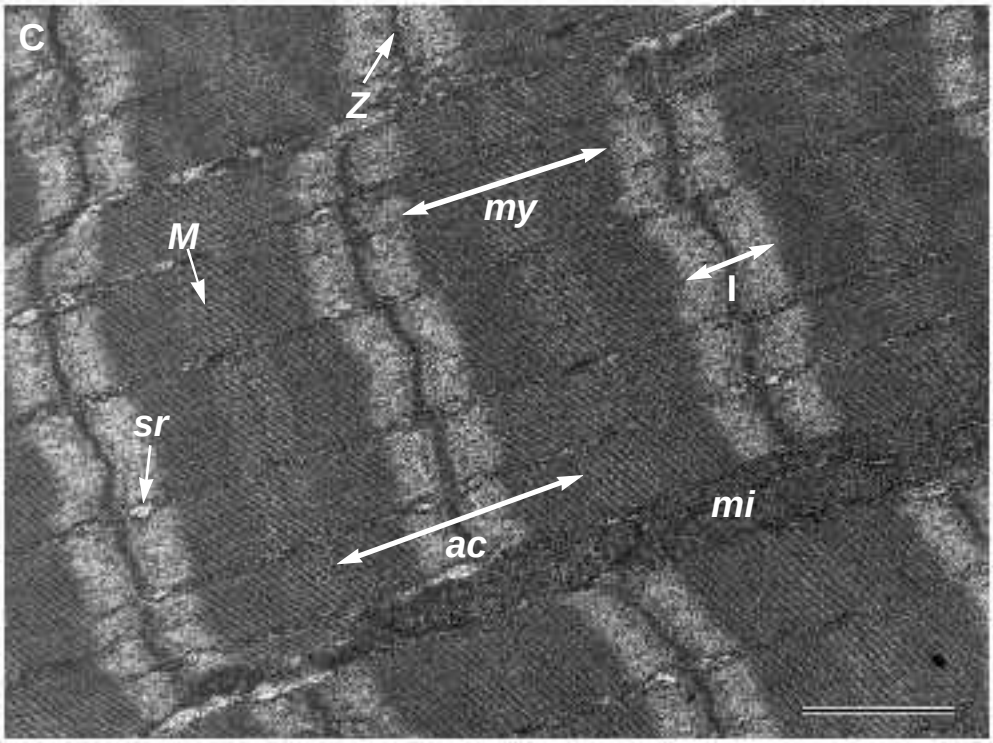
C
z
my
M
I
sr
mi
ac

actin filaments measured approximately 1.8 μm (a larger sample from several experimental fibers will be described below). Numerous mitochondria are located between individual myofibrils (Fig. 1C).

Actin and myosin filaments are arranged in a hexagonal lattice (Fig. 2B). Each thick filament is surrounded by six thin filaments, and each thin filament faces two thick filaments. This packing structure gives a ratio of three thin filaments for each thick filament.

The cytoplasmic compartment of these cardiac fibers is rich in mitochondria (Fig. 2C); the ground substances of the cytoplasm has a granular appearance in the electron microscope (Fig. 2C). The extracellular matrix (ECM) covering the surface of these fibers ranges from about 100 to 400nm in thickness. In the example shown in Fig. 2C, the ECM is about 250nm thick.

Physiological range of loading frequencies, pressures and sarcomere lengths

The physiological range of loading frequencies and pressures was evaluated from transcardiac pressure recordings (Fig. 3). Ventilating crabs that moved slowly in the recording tank generated transcardiac pressure differences of approximately 1000Pa at a beat frequency of approximately 1Hz (Fig. 3A). The corresponding power spectrum (power spectral or autospectral density function) of the entire time series (Fig. 3C) clearly shows (1) that the heart beats with a fundamental frequency of 1Hz; (2) that most of the power is contained at that fundamental frequency, since the autospectral density drops more than 20dB to the harmonic frequencies; and (3) that changes in the beat frequency are very small, as indicated by the sharpness of the peak at the fundamental frequency. In Fig. 3B, a pressure record from a quiescent crab with reduced ventilation is shown. Interestingly, during periods of reduced circulatory demand, intracardiac pressure is reduced and the heart intermittently stops beating. However, as shown on the corresponding power spectrum (Fig. 3D), the cardiac beat frequency remains close to 1 Hz. The intracardiac pressure under this condition drops to approximately 500Pa. For these organisms, cardiac output appears to be regulated by bouts of cardiac activity with a conservative intra-bout frequency.

The physiological range of sarcomere length is based on two different microscopical observations. First, sarcomere length measurements from *in situ* fixations of cardiac tissue indicated that the physiological sarcomere length is close to 4.0 μm (Fig. 2). This

Fig. 2. Fine structure of myofibrils from the heart muscle of *Cancer magister*. (A) Detailed electron micrograph of a single sarcomere from a longitudinal section. Actin and myosin filaments (*my*) are clearly visible. The myofibrillar surface is ensheathed in a fenestrated cisternal and tubular sarcoplasmic reticulum (*sr*). At the level of the H-zone, the sarcoplasmic reticulum is closely associated with T-tubules in dyad and triad configurations (*d*). Scale bar, 1 μm. (B) High-magnification cross section through a myofibril. The regular pattern of thick or myosin (*my*) and thin or actin (*ac*) filaments shows the packing ratio of three thin for each thick filament. Scale bar, 250nm. (C) Transverse section of a cardiac fiber showing the ultrastructural organization at the fiber edge. Directly beneath the cell membrane (*cm*), numerous large mitochondria (*mi*) are found in the granular cytoplasm (*c*). The extracellular matrix (*ecm*) is located directly above the cell membrane; it is about 250nm thick. Scale bar, 1 μm.

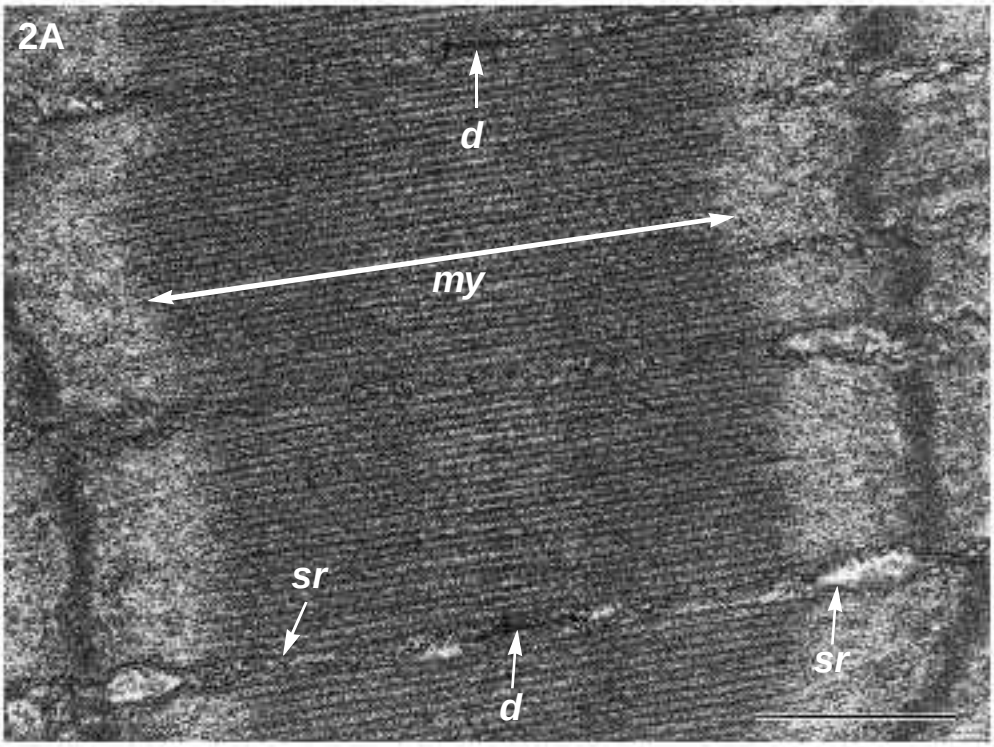
2A
d
my
sr
d
sr

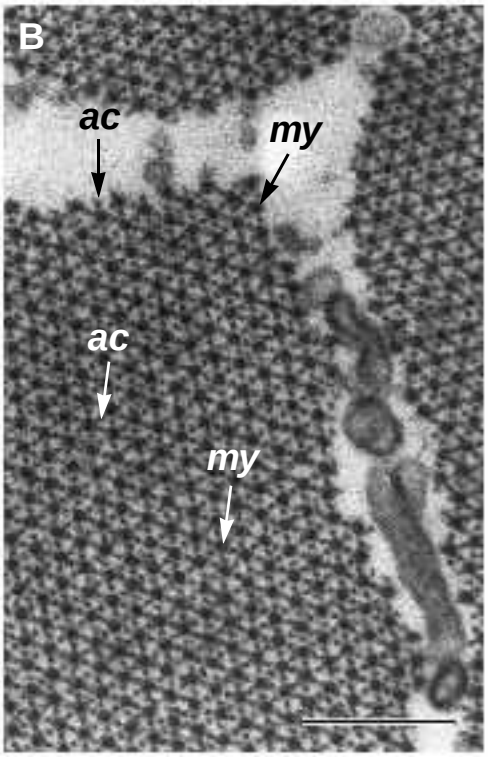
B
ac
my
ac
my

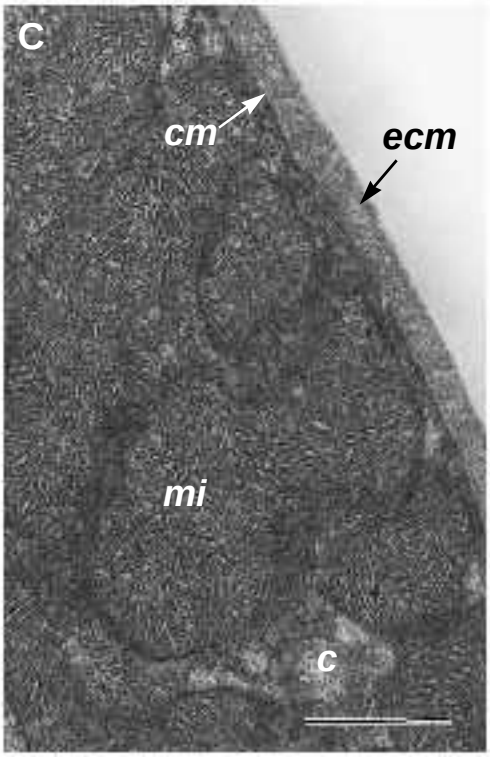
C
cm
ecm
mi
c

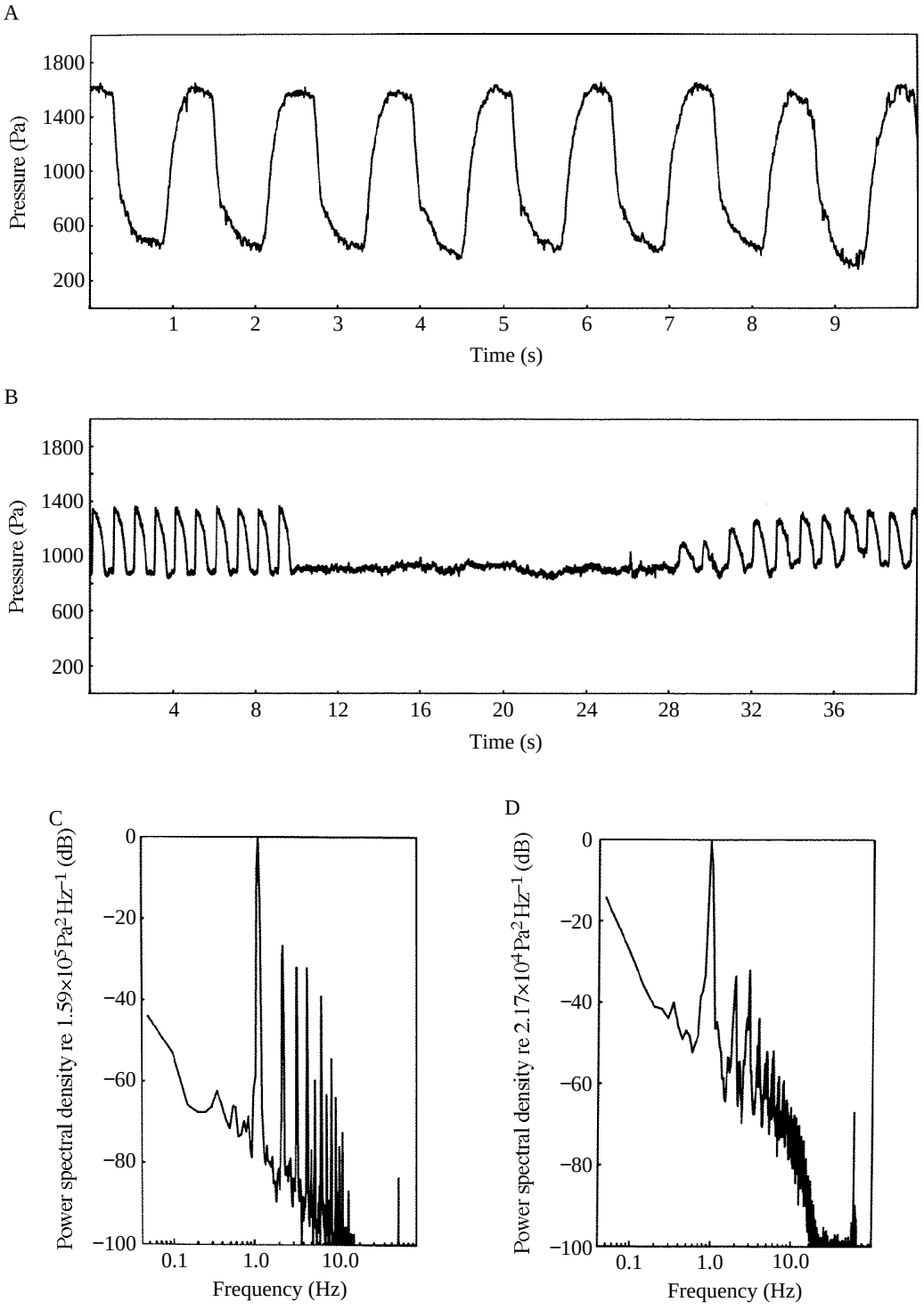
A
Pressure (Pa)
1800
1400
1000
600
200
1
2
3
4
5
6
7
8
9
Time (s)
B
Pressure (Pa)
1800
1400
1000
600
200
4
8
12
16
20
24
28
32
36
Time (s)
C
Power spectral density re 1.59×10⁵Pa²Hz⁻¹ (dB)
0
−20
−40
−60
−80
−100
0.1
1.0
10.0
Frequency (Hz)
D
Power spectral density re 2.17×10⁴Pa²Hz⁻¹ (dB)
0
−20
−40
−60
−80
−100
0.1
1.0
10.0
Frequency (Hz)

Fig. 3

measurement is likely to represent the lower end of the range of sarcomere length, since the hearts always contracted upon the injection of fixative. A second estimate comes from the measurement of the myofilament length of experimental cells. Actin and myosin length estimates from transmission electron microscopy of five experimental cells (Table 2) indicate that 100% myofilament overlap occurred in the sarcomere length range 3.8–4.0 μm. Thus, the lower end of the physiological range of sarcomere lengths is expected to be close to 4.0 μm.

The *in situ* strain of cardiac fibers can be estimated from the thermodilution experiments of D. D. Jorgensen (personal communication). This work shows that, during a typical heartbeat, 20–30% of the cardiac volume is ejected. During sustained exercise on a treadmill, this fraction might rise to close to 50%. These conditions yield tissue strains of about 10% and 20% respectively.

These results, taken together, strongly suggest that the heart of *Cancer magister* beats at 1Hz and does not modulate its beat frequency. The sarcomere length during a 'normal' beat cycles through a 10% length excursion from about 4.0 to 4.4 μm. Under strong circulatory demand, this strain is likely to increase to 20%. These findings imply that physiological strain rates fall into a range of strain rates from 0.5 to 1.2rad s^{-1}. The intracardiac systolic-to-diastolic pressure difference is approximately 1000Pa.

Mechanical properties

Mechanical properties of single cardiac fibers

Several general trends, illustrated for an individual fiber (Figs 4 and 5), emerge. The total stiffness (or complex modulus) of all fibers increases by approximately two orders of magnitude from roughly 0.01 to 1MPa over the sarcomere length range from about 3.8 to 6.0 μm. In addition, the total stiffness increases weakly (two- to threefold) at each sarcomere length over the strain rate range 0.01–5rad s^{-1}. The elastic modulus expressed

Fig. 3. Cardiac pressure. (A) Transcardiac pressure was recorded from an unrestrained crab that was allowed to move around freely. The time series shown was recorded from a crab that moved slowly in the recording aquarium and was ventilating strongly. The slow transient shifts in the baseline pressure are due to changes in the vertical position of the animal. Data were collected at 200 points per second. The entire record was 16384 points (81.9s) long; only 10s of the total record is shown. (B) This pressure record was recorded from a crab that was resting in the recording aquarium and had significantly reduced its ventilatory activity. The systolic–diastolic pressure difference is only about 500Pa and for a period of about 15 s the heart ceased to beat. (C) Power spectral density function of the cardiac pressure record shown in A. The spectral density was referenced to 1.59×10^{5} Pa^{2} Hz^{-1}. Most of the power of the signal is contained in the relatively narrow band at 1Hz; the next harmonic frequency at 2.0Hz contains only about 5% of the signal power. The background noise drops off fairly steeply with frequency, as is to be expected from a strain-gauge-type pressure transducer. There is no signal component below 1Hz. (D) Power spectral density function of the pressure record shown in B. The spectral density was referenced to 2.17×10^{4} Pa^{2} Hz^{-1}. Again the fundamental beat frequency is at 1Hz and has a narrow peak. The harmonics at 2 and 3Hz account for approximately 2% of the signal. Thus, under low circulatory loading, the beat frequency of the *Cancer magister* heart does not change, cardiac pressure declines from about to 1000Pa to 500Pa, and the heart might temporarily stop beating.

Table 2. *Lengths of myofilaments*

	Myosin			Actin		
Cell	Length (μm)	S.D.	*N*	Length (μm)	S.D.	*N*
1	3.29	0.155	24	1.97	0.121	24
2	3.58	0.307	18	2.07	0.252	17
3	3.05	0.131	21	1.77	0.064	29
4	3.23	0.160	25	1.84	0.133	29
5	3.13	0.247	18	1.71	0.166	17

as a function of sarcomere length and strain rate follows a similar pattern to the complex modulus. The absolute values of the elastic modulus at a given sarcomere length and strain rate are usually no more than a factor of two lower than those observed for the complex modulus. An interesting pattern, however, emerges for the viscous behavior of these fibers. At low strain rates, the viscous modulus is nearly an order of magnitude lower than the elastic modulus at the same sarcomere length. However, at these low sarcomere lengths, the viscous modulus rises very steeply with strain rate (about 10-fold over the strain rates used here) and approaches, or even exceeds, the magnitude of the elastic modulus at the higher strain rates used in these experiments (0.5–5rad s^{-1}). At relatively longer sarcomere lengths, the viscous modulus increases only weakly or even falls slightly.

The behavior of individual moduli as a function of sarcomere length and strain rate has an interesting effect on the relative energy dissipation [$\tan\delta=(E''/E')$; Fig. 5]. For each single fiber, the relative energy dissipation reaches quite large values (0.6–1.0) for shorter sarcomere length (<4.5 μm) and strain rates above 0.5rad s^{-1}. This range of sarcomere lengths and strain rates for which high values of energy dissipation occur corresponds to the physiologically relevant range.

Two general results emerge from these observations and are consistent with previous results on shrimp extensor cells (Meyhöfer and Daniel, 1990). Single cardiac fibers from the heart of the crab *Cancer magister* are viscoelastic, and their relative energy dissipation is large for physiologically relevant sarcomere lengths and strain rates, but considerably smaller outside this range. Such a high value for the relative energy dissipation indicates that as much as half of the mechanically imparted energy is dissipated viscously.

Strain rate versus *frequency*

The modulus of a linearly viscoelastic material depends on the frequency of the length perturbation when infinitesimal strains are used (Fung, 1981; Ferry, 1980). For finite-amplitude perturbations applied to non-linear viscoelastic materials, however, the instantaneous value of the stress depends not only on the instantaneous strain value but also on the entire history of the strain, which includes all of its derivatives (Christensen, 1982). Thus, to a first-order approximation, we might expect that the mechanical properties of a non-linear viscoelastic material would depend on the rate of strain and

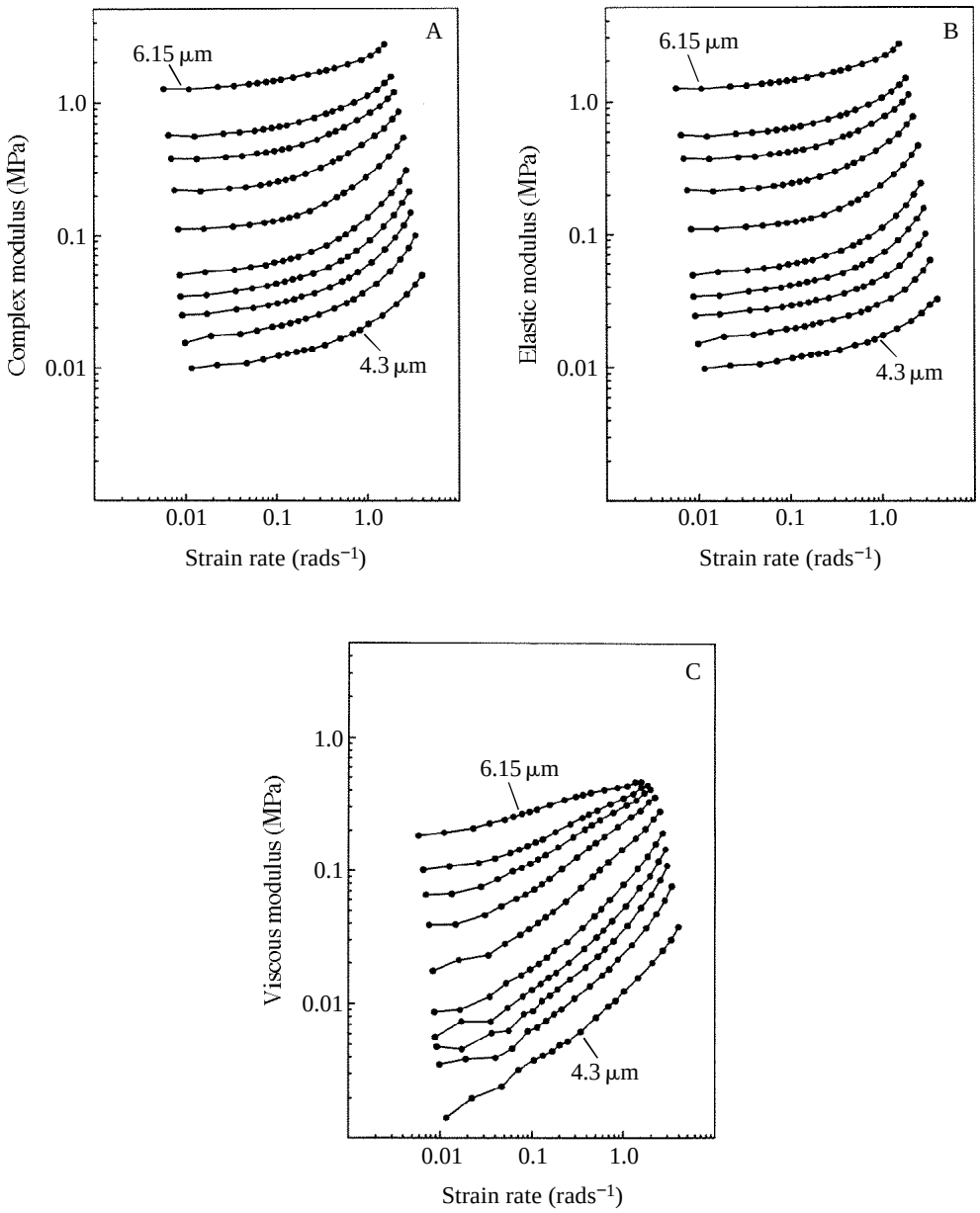

Fig. 4. Dynamic mechanical properties of a single cardiac fiber. The complex (A), elastic (B) and viscous (C) moduli are plotted as functions of strain rate and sarcomere length. Each circle indicates the location of a measured data point; data points for the same sarcomere length are connected by a straight line. All data were collected from the same single cardiac fiber. The sarcomere lengths (increasing modulus) were 4.3, 4.5, 4.65, 4.8, 5.1, 5.15, 5.45, 5.65, 5.85 and 6.15 μm. Note the logarithmic scales. All moduli increase strongly with sarcomere length. The viscous modulus at short sarcomere lengths exhibits the largest dependence on strain rate.

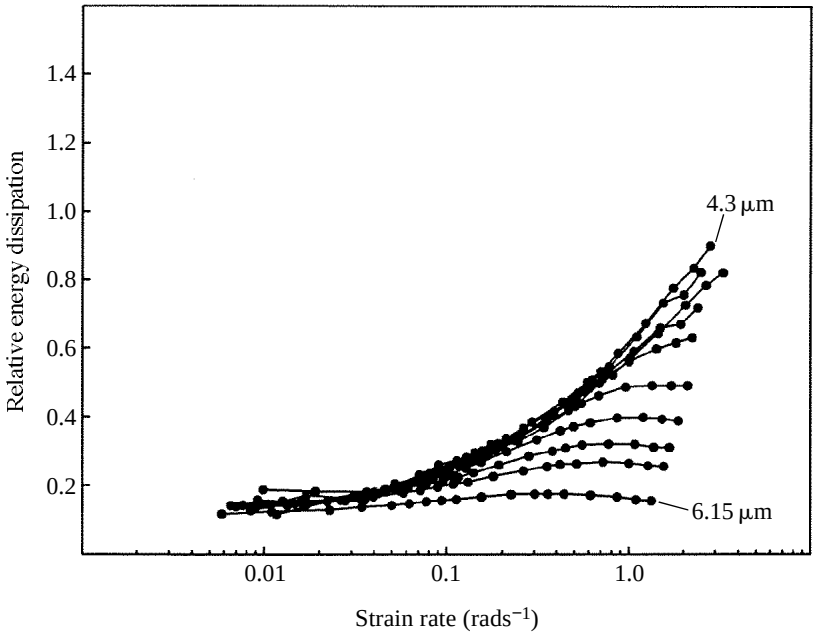

Fig. 5. Relative energy dissipation of a single cardiac fiber. The relative energy dissipation for the same fiber as in Fig. 4 is plotted as a function of strain rate and sarcomere length. Data points from the same sarcomere length are connected by straight lines. Sarcomere lengths increase with declining relative energy dissipation and are the same as listed for Fig. 4.

would not simply be frequency- or amplitude-dependent. Indeed, observations on large-amplitude deformations of tendon and skin support this idea (Wainwright *et al.* 1976). To determine experimentally whether this first-order approximation applies, a few fibers were oscillated through the same set of frequencies with two distinct strain amplitudes differing by about one order of magnitude. In Fig. 6 the phase (δ) from such an experiment is plotted as a function of both frequency and strain rate. The phase variable was chosen for this analysis because it is the most sensitive to changes in strain rate and frequency. The results of these experiments show that nearly identical results arise from fixed values of strain rate and not from fixed values of frequency (Fig. 6).

Analysis for non-linearity

The non-linearity (distortion) for one particular experiment is analyzed by first estimating the autospectral density of the mechanical response (force signal) at the fundamental and harmonic frequencies. Following Bendat and Piersol (1986), the total power is then calculated from:

$$P_t = [\,|G_{xx}(mf_k)|^2]^{1/2} \qquad \{m = 1, 2, 3,..., 7\}, \tag{18}$$

where

$$k = n_w/T. \tag{19}$$

All variables are defined the same way as in the Materials and methods section, and n_w is

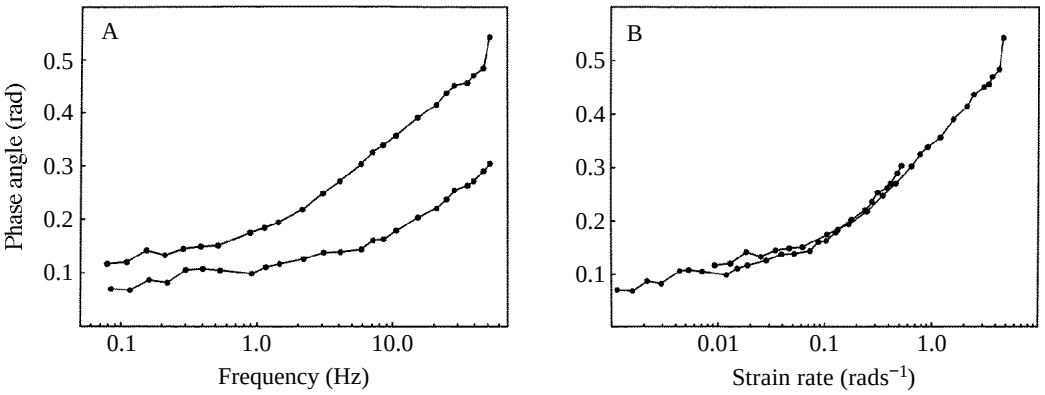

Fig. 6. Comparison between frequency (A) and strain rate (B). The phase angle (δ) of two different sets of sinusoidal experiments is plotted as a function of frequency and strain rate. For both experiments, the same fiber was oscillated at the same 25 frequencies, but in the first experimental run the mean strain amplitude was about 0.36%, whereas in the second run it was close to 3.6%. Data points from the same experimental run (same strain amplitude) are connected by straight lines. The mean sarcomere length of the fibers was kept constant at 4.3 μm for both experiments.

the integer number of sine waves in the record of length T. Since the power vanished very quickly after the fourth harmonic, only the fundamental (m=1) and the first six harmonic frequencies (m=2 to m=7) were included in the calculations. The relative amplitudes of the fundamental and harmonics were then estimated from:

$$A_m = [G_{xx}(mf_k)/P_t]^{1/2} . \tag{20}$$

The relative amplitude of the force (here A_1 or in general the output signal) represents the linearity of the signal. In addition, I estimated the distortion or non-linearity in the force signal by using the above-calculated relative amplitudes:

$$L = A_1 , \tag{21a}$$

$$D = \left[\sum_{m=2}^{7} |A_m|^2\right]^{1/2} . \tag{21b}$$

In Fig. 7 the linearity (L), distortion (D) and relative amplitudes of the harmonics (A_2–A_5) are shown as a function of strain rate for an entire experimental run. This particular experimental run was chosen because the strain in these experiments was 0.89%, which was slightly above the mean of 0.8771±0.0321% (N=1014) for all experiments reported in this paper. Most of the non-linearity is accounted for by the first two harmonic amplitudes (1 and 2 in Fig. 7A). The total distortion does not exceed 0.08. Thus, the total non-linear power is less than 0.64% and the linearity is better than 99.6%. On the basis of these measurements, I conclude that the perturbations used for the work reported here were sufficiently small to justify a linear analysis.

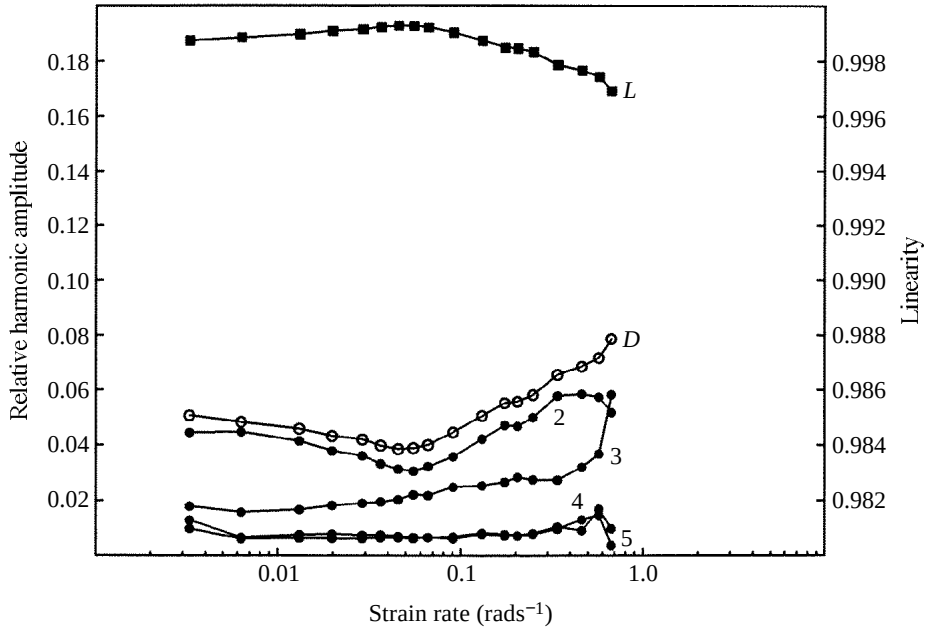

Fig. 7. Analysis of nonlinearity. The relative amplitudes of the second to fifth harmonic (2–5) and total harmonic distortion (*D*, open circles) are depicted as a function of strain rate for a typical experimental run. For these measurements, the magnitude of the distortion is indicated by the relative harmonic amplitude scale on the left-hand side of the figure. The total harmonic distortion reaches a maximum of about 0.08 at close to 1rad s^{-1}. The calculated linearity as a function of strain rate is also plotted in this figure (*L*, filled squares). It reaches its minimum of 0.996 at 1rad s^{-1}, indicating that the signal is linear. The scale for linearity is given on the right-hand side of the figure. The sarcomere length was 4.8 μm and the mean strain amplitude for the sinusoidal perturbations in this experiment was 0.89%.

Average mechanical behavior of single cardiac fibers

Although several distinct trends emerged from the analysis of single fibers, an appreciable variability between individual fibers was also apparent. Accordingly, I pooled data from 10 single cardiac fiber experiments to quantify such trends. First, mechanical properties were sorted, according to sarcomere length and strain rate, into small bins of each variable. The mean and standard deviation of each mechanical measure were determined and data from the same range of strain rates were plotted against sarcomere length (Fig. 8). The strain rate bins were selected to contrast the mechanical behavior of the fibers inside the range of physiologically relevant loading with that outside. For the three ranges of strain rates, the complex and elastic moduli, plotted on a logarithmic scale, increase approximately linearly over the sarcomere length from 3.8 to 6.2 μm, indicating a possible exponential or power relationship between these moduli and sarcomere length. The average total stiffness (complex modulus) of these fibers rises from roughly 0.01MPa at 3.8–4.0 μm to 1MPa at 6.0 μm at the lower strain rates (0.001–0.5rad s^{-1}); the same moduli are about two- to threefold larger at higher strain rates (up to 10rad s^{-1}).

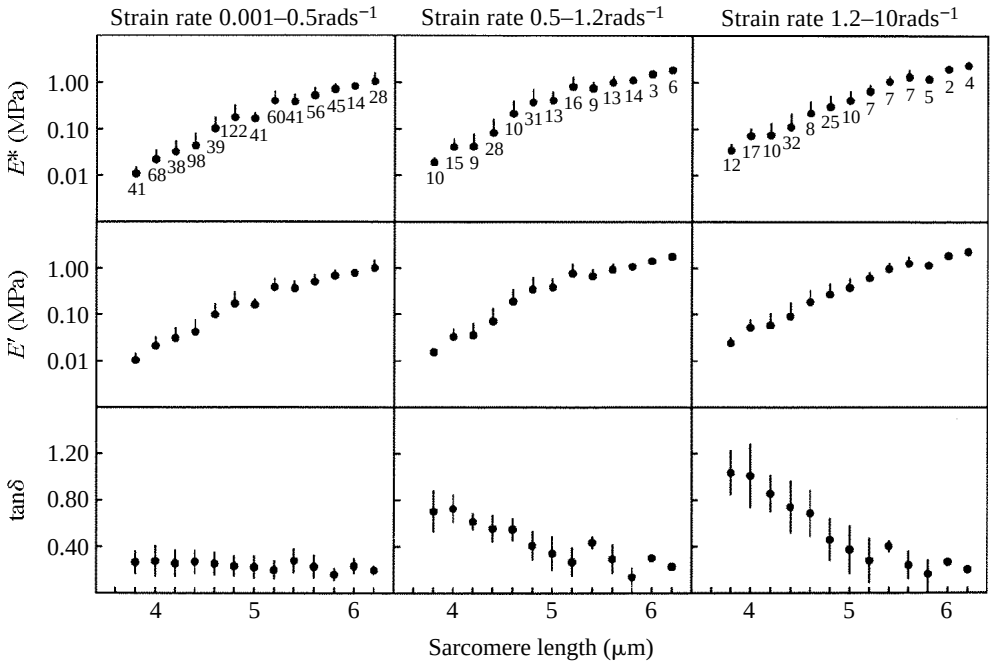

Fig. 8. Average mechanical behavior of single cardiac fibers. The complex modulus (E^*), elastic modulus (E′) and relative energy dissipation (tanδ) are plotted for three strain rate bins (0.001–0.5, 0.5–1.2 and 1.2–10rad s^{-1}) as a function of sarcomere length. The second bin encompasses the physiological range of strain rates, whereas the other two bins are outside this range. Data from 10 cells were pooled for this analysis. For the moduli, one standard deviation is drawn as a vertical line upwards from the mean. The number of points in each mean is specified below each mean. Moduli are plotted on a logarithmic scale and change by about two decades over the sarcomere length range from 4 to 6 μm. The behavior of all moduli in the different strain rate bins is approximately similar. The magnitude of the relative energy dissipation, however, changes from strain rate bin to bin; in the physiological range of strain rates and sarcomere lengths (4.0–4.4μm), the average relative energy dissipation is about 0.6.

The ratio of viscous to elastic moduli (tanδ) shows an interesting dependence on sarcomere length and strain rate. At low strain rates (<0.5rad s^{-1}), the relative energy dissipation is independent of sarcomere length and is low, with values ranging between 0.1 and 0.2. However, at higher strain rates, the relative energy dissipation depends on sarcomere length. It can reach values near 1.0 at 3.8–4.2 μm sarcomere lengths and drops to values of approximately 0.15 at sarcomere length of 5.0 μm and above. In the relatively narrow range of physiological sarcomere lengths and strain rates (0.5–1.2rad s^{-1}, 4.0–4.4 μm), the relative energy dissipation reaches an appreciable value of about 0.5–0.7 (Fig. 8, middle column).

Mechanical response surfaces for single cardiac fibers

The results presented in the previous sections show that the mechanical responses of single cardiac fibers depend on both sarcomere length and strain rate and, therefore, form

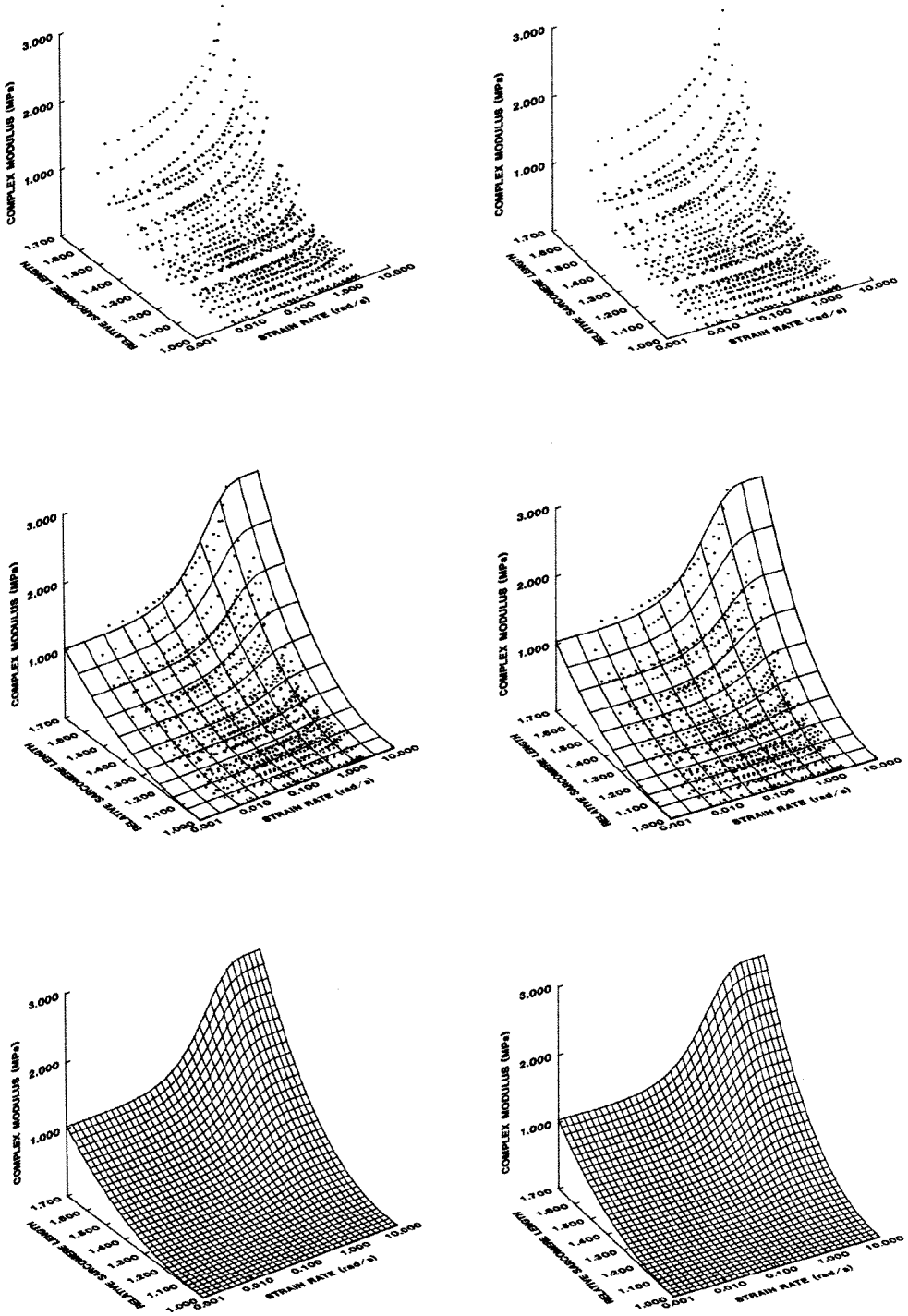
COMPLEX MODULUS (MPa)
3.000
2.000
1.000
RELATIVE HUMIDITY (%)
1.700
1.600
1.500
1.400
1.300
1.200
1.100
1.000
STRAIN RATE (rad/s)
0.001
0.010
0.100
1.000
10.000

Fig. 9

a complex three-dimensional response surface. To evaluate and quantify this response surface better, mechanical data were fitted to descriptive equations (equations 14 and 15) and then plotted together with the model as stereopairs. As described in the Materials and methods section, I chose one model to represent the total stiffness and another model to described the relative energy dissipation. In Fig. 9, stereopairs of three-dimensional plots relating the total stiffness to relative sarcomere length and strain rate are shown. Note that relative sarcomere lengths of 1.0 and 1.7 are equivalent to absolute sarcomere lengths of 3.7 μm and 6.29 μm, respectively (see equation 17). The relationship between the relative energy dissipation and the independent variables sarcomere length and strain rate is depicted in Fig. 10.

Inspection of the stereopairs (Figs 9 and 10) reveals the same general trends described above. (1) The total stiffness of single cardiac fibers rises steeply with sarcomere length and weakly with strain rate (Fig. 9). (2) The relative energy dissipation depends strongly on sarcomere length and strain rate (Fig. 10).

The response surfaces fitted to the data demonstrate that the relative energy dissipation exceeds values of 1.0 for low sarcomere lengths (1.0–1.2 relative sarcomere length) and high strain rates (1–10rad s^{-1}) (Fig. 10). From these values, the relative energy dissipation declines smoothly with increasing sarcomere length and with decreasing strain rates (Fig. 10). In the predicted physiological range of sarcomere lengths and strain rates, the response has a steep gradient, especially with respect to strain rate. Note, however, that the gradient with respect to sarcomere length at the largest strain rate appears to be underestimated because of the lack of data points at large sarcomere lengths and high strain rates. At strain rates below 0.1rad s^{-1}, the response surface is essentially flat for all sarcomere lengths. The response surface fitted to the relative energy dissipation data suggests the possible existence of a maximum. However, this finding should be treated with great care. The response surface contains too few data with strain rates beyond the possible maximum, and part of the response surface extends slightly beyond the region evaluated by data points.

The steep increase of the total stiffness response surface as a function of sarcomere length can be approximated by a power function with an exponent of about 2.3 (Fig. 9; equation 14). The total stiffness also increases with strain rates above 0.1rad s^{-1}. Again, the steepest change of the total stiffness with respect to strain rate falls into the physiologically relevant range. The model predicts a total stiffness of about 45kPa for a

Fig. 9. Mechanical response surface of single cardiac fibers: linear three-dimensional plot of the total stiffness as a function of sarcomere length and strain rate. The total stiffness of 10 single cardiac fibers and the model fitted to the data are plotted in stereopairs as a function of relative sarcomere length (referenced to 3.7 μm) and strain rate. 1014 data points were used for each these plots. The stereopair at the top of the figure shows only data, the one in the middle includes a coarse grid of the model, to allow a comparison between the data and the model, and the bottom pair shows the model displayed with a finer grid. The following variables were obtained when the model (equation 14) was fitted to the data using the least-squares method: a=6555.6Pa, b=52.753Pa, c=2.3252, d=1.5713 and e=1.2499(rad s^{-1})$^{-1}$. The good fit of the model to the data is indicated by the r^2 value of 0.899 and the F-value of 1269.0 (5 and 1009 degrees of freedom).

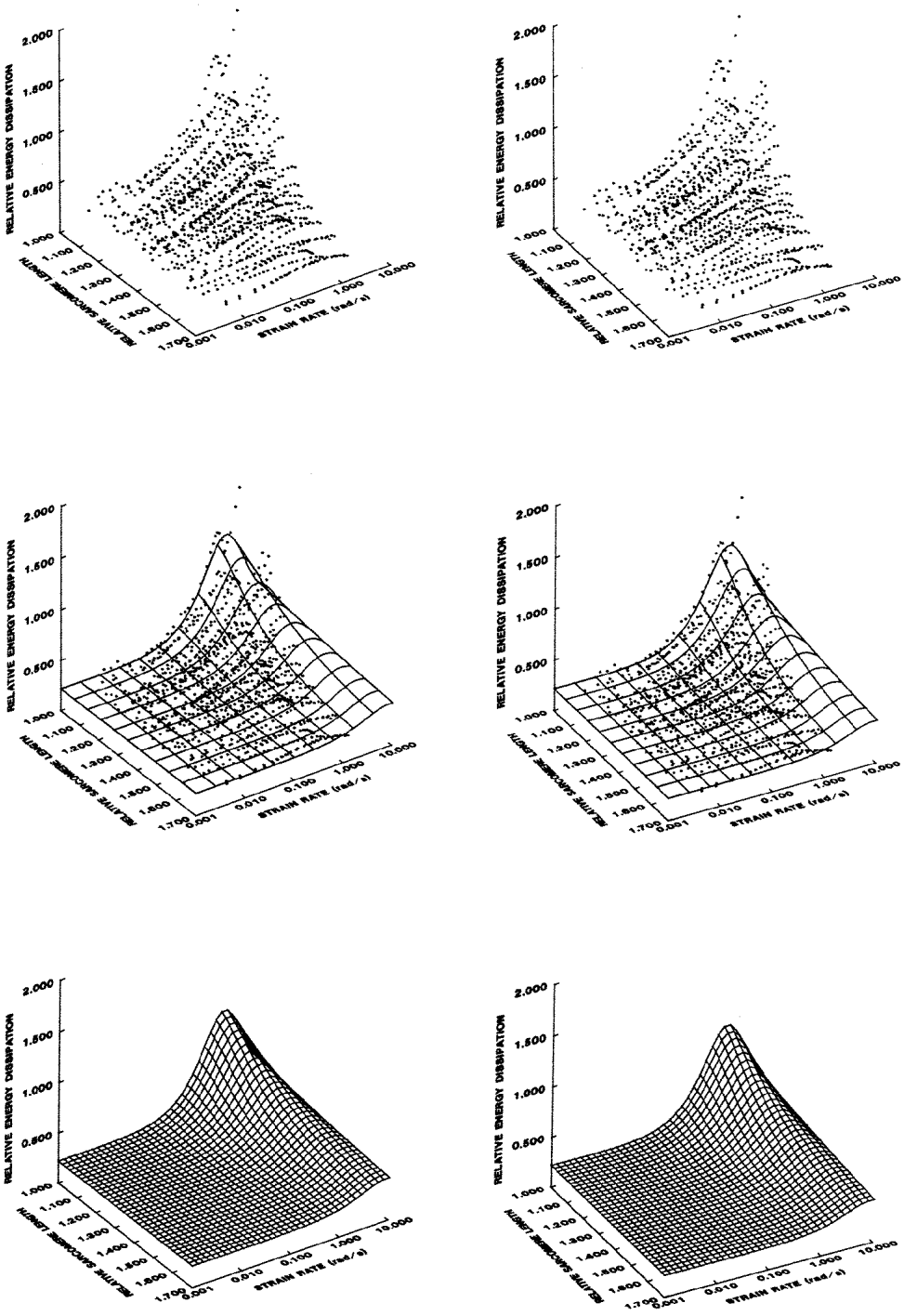
RELATIVE ENERGY DISSIPATION
2.000
1.500
1.000
0.500
RELATIVE SACCHARIDE LENGTH
1.000
1.100
1.200
1.300
1.400
1.500
1.600
1.700
STRAIN RATE (rad/s)
0.001
0.010
0.100
1.000
10.000

Fig. 10

single cardiac fiber at a sarcomere length of 4.2 μm, deforming at a strain rate of 0.6rad s^{-1}. Values of all fitting variables are summarized in the respective figure legends.

The complex modulus and relative energy dissipation models provide good fits to their respective mechanical measurements. This conclusion is strongly supported by a goodness-of-fit analysis of the overall regression. The observed *F*-ratios exceed the selected percentage point of the *F*-distribution [$F_{0.001(1),5,1009} \approx 4.10$, Zar 1984] by more than 100-fold (see legends of Figs 9 and 10), indicating that the model is a highly significant predictor in the sense that the range of response values predicted by the models is extremely large compared with the standard error of the response (Draper and Smith, 1981). In addition, the r^2-values for the complex modulus model and relative energy dissipation model are large with respective values of 0.899 and 0.928. Therefore, about 90% of the variability in the complex modulus and relative energy dissipation is explained or accounted for by the fitted models. The stereopair plots also establish that the residuals achieve approximate homoscedasticity. In this context, it is important to remember that the number of individual cells used in this analysis is relatively small whereas the total number of data points is large.

Relationship between mechanical data and the extracellular matrix

The role of the extracellular matrix as a determinant of the passive mechanical behavior of single cardiac fibers was investigated by relating the volume fraction of ECM to a measure of their mechanical properties (Table 3). In Fig. 11 the typical ultrastructural appearance of experimental fibers is shown. The thickness of the ECM was measured from electron micrographs as depicted in Fig. 11B,C. I chose to relate the ECM volume fraction to the total dynamic stiffness at 5.6 μm and 2Hz, because this required the least interpolation between measurements. The strain rates for these measurements range from 0.06 to 0.08rad s^{-1}.

Estimates of the mean thickness of the extracellular matrix for individual fibers vary between 178 and 269nm and do not correlate well with the total stiffness of fibers. It appears, therefore, that this measurement cannot account for the nearly 10-fold variation in total stiffness. However, since fiber dimensions are also quite variable, the estimates of the ECM volume fraction exhibit a different pattern (Fig. 12). The following relationship emerges: a larger ECM volume fraction correlates with a stiffer fiber. Regression analyses on both the mean values and all measurements (see Fig. 12 legend) suggest that a linear relationship exists between the ECM volume fraction and the total dynamic stiffness.

Fig. 10. Mechanical response surface of single cardiac fibers: three-dimensional plot of the relative energy dissipation as a function of sarcomere length and strain rate. The relative energy dissipation (tanδ) depends on sarcomere length and strain rate and reaches its largest values at short sarcomere lengths and high strain rates (note the reverse relative sarcomere length axis). The least-squares best fit for the relative energy dissipation model (equation 15) produced the following values for variables and measures of goodness of fit: f=0.23168, g=0.8205(rad s^{-1})$^{-1}$, h=0.1808(rad s^{-1})$^{-2}$, k=0.012669(rad s^{-1})$^{-1}$, l=0.02459, r^2=0.928, F=739.61, d.f.=5 and 1009, N=1014. Notice that the model predictions of high values of tanδ at longer sarcomere lengths and the highest strain rates extend over the data domain.

Table 3. *Relationship between fiber geometry, dynamic stiffness and extracellular matrix (ECM)*

Cell	Area (μm^2)	Perimeter (μm)	E^* (MPa)	ECM thickness (nm) Mean	ECM thickness (nm) S.D.	V_{ECM} (%) Mean	V_{ECM} (%) S.D.	*N*
1	1496	195	0.66	178.3	40.55	2.32	0.52	41
2	1582	263	2.95	238.9	75.34	3.97	1.25	46
3	8431	761	1.26	268.5	78.69	2.42	0.71	40
4	6944	548	0.34	195.7	59.64	1.55	0.47	66
5	1175	149	0.80	189.7	51.24	2.40	0.65	22

The dynamic stiffness for all five cardiac fibers analyzed was referenced to a sarcomere length of 5.6 μm and a frequency of 2Hz.

N is the number of electron microscope measurements of the thickness of the ECM and the volume fraction of the ECM (V_{ECM}) is given as a percentage.

Discussion

This paper describes the dynamic mechanical properties of passive single cardiac fibers of the Dungeness crab *Cancer magister* for a wide range of sarcomere lengths and strain rates, including those that are physiologically relevant. These measurements revealed strong viscoelastic behavior similar to that reported for shrimp extensor cells (Meyhöfer and Daniel, 1990). Cardiac fibers from *Cancer magister* are therefore not purely elastic, as has tacitly been assumed in most studies on the passive mechanics of skeletal and cardiac fibers (for example, Magid and Law, 1985; Fabiato and Fabiato, 1978; Fish *et al.* 1984).

Several main findings arise from the data: (1) the elastic and viscous moduli of these cardiac fibers depend upon both sarcomere length and strain rate; (2) their relative energy dissipation is large in the physiologically relevant range of sarcomere lengths and strain rates; and (3) there is a positive and statistically significant correlation between the relative amount of ECM and the total dynamic stiffness. The implications that these

Fig. 11. Ultrastructure of single experimental cardiac fibers from *Cancer magister*. (A) Detailed electron micrograph of a longitudinal section showing the sarcomere structure of a fiber that had been used for dynamic mechanical experiments. The A-band (*my*) and I-band (*I*) as well as the Z-line (*Z*) and M-line (*M*) are well preserved, allowing the measurements of sarcomere length and the length of the myofilaments. The effectiveness of the Chaps skinning procedure is illustrate by the disruption of the sarcoplasmic reticulum (arrow). Scale bar, 1 μm. (B) Transmission electron micrograph of a cross section of the edge of a single cardiac fiber. The extracellular matrix (*ecm*) is well preserved in experimental fibers (see also C) and hence the thickness can be measured from such material. Note the disruption of all membrane systems; the cell membrane has virtually disappeared, and the large mitochondria usually found directly beneath the cell membrane (compare with Fig. 2C) have been destroyed. Scale bar, 1 μm. (C) Transmission electron micrograph of a longitudinal section of an experimental fiber, showing good structural preservation of the myofibrillar filaments and the extracellular matrix. The sarcomere length in this fiber was approximately 6.0 μm. *A*, A-band; *I*, I-band. Scale bar, 2 μm.

results have for cardiac function are discussed below and related to my stability hypothesis. First, however, I will compare the morphology and ultrastructure of the cardiac fibers of *Cancer magister* with those of related animals. I then ask if these measured dynamic mechanical properties of the cardiac preparation appear reasonable by

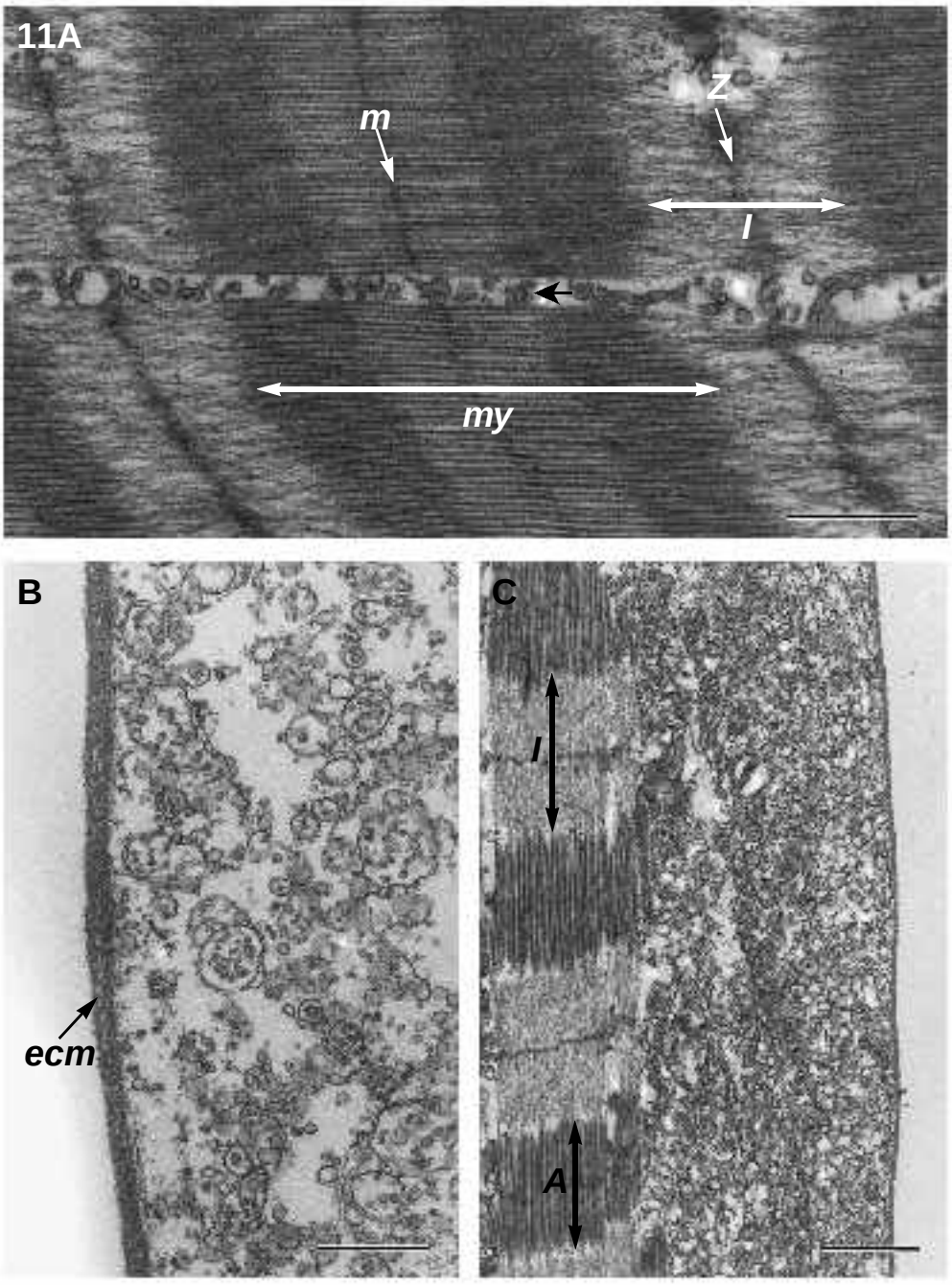

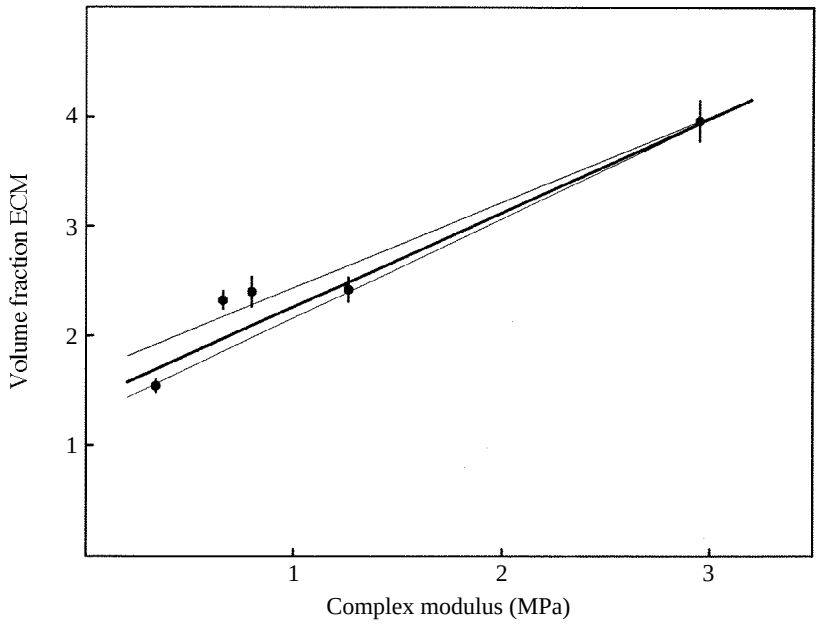

Fig. 12. Relationship between the volume fraction of ECM and the complex modulus. The volume fraction of extracellular matrix (ECM, expressed as a percentage) is plotted for five fibers as a function of the complex modulus (5.6 μm, 2.0Hz). The standard error of the mean is indicated by the vertical lines. The linear fit to all data points (not the mean) is shown by the thick lines, and the 95% confidence interval is shown by the thin lines (r^2=0.916, F=242.8, P<0.001). A regression on the mean values is also highly significant (r^2=0.936, F=43.8, P≈0.007).

comparing them with previous mechanical measurements on other cardiac muscle fibers. I conclude this paper by examining the energetic consequences of these mechanical properties for cardiac function and discuss the possible structural basis of the above data.

Morphology and ultrastructure of cardiac muscle fibers

The ultrastructure of muscle fibers from the heart of the crab *Cancer magister* closely resembles that of crustacean skeletal fibers: myofibrils exhibit the characteristic cross-striation pattern of bands and lines, numerous mitochondria populate the cytoplasmic compartment, and an extensive membrane system of tubules and sarcoplasmic reticulum is present in these fibers. Similar observations have been reported for cardiac fibers from the lobster *Homarus americanus* (Anderson and Smith, 1971; Smith and Anderson, 1972), the horseshoe crab *Limulus polyphemus* (Sperelakis, 1970) and a few other crustaceans (for a summary of much of this work, see Sanger, 1979; Hoyle, 1983). More importantly for these experiments, single cardiac fibers in crustaceans, while being considerably smaller than their skeletal counterparts, are huge compared with vertebrate single cardiac fibers and can therefore be dissected mechanically.

The resting sarcomere length of *Cancer magister* cardiac fibers was estimated to be between 3.8 and 4.0 μm on the basis of sections of fixed tissue *in situ* and myofilament

length measurements from experimental fibers. In this context, it is important to remember that a considerable degree of variability, reflected by the error (standard deviation) of the myofilament lengths, was associated with these measurements. Such a degree of variability of a morphological characteristic is not uncommon for crustacean muscle (Atwood, 1973; Sanger, 1979; Franzini-Armstrong *et al.* 1986). This estimate of the resting sarcomere length falls approximately into the middle of the range (1.8–6.6 μm) of sarcomere lengths observed for other crustacean cardiac fibers (Hoyle, 1983) and therefore does seem not unreasonable. Unfortunately, it is not clear whether the observed uncertainty is based on variability between single fibers, between individual animals, or both, because each experimental fiber was dissected from a different animal.

Some important morphological features deviate from the pattern commonly observed for crustacean skeletal fibers: the myofibrillar volume fraction is small in *Cancer magister* cardiac fibers (only about 50%) and under physiological conditions these fibers are separated by appreciable distances (40–70 μm is a common range). Because of the limited ultrastructural information available for crustacean cardiac fibers, it is unclear whether these morphological characteristics are unique to cardiac fibers from *Cancer magister*. In contrast to Anderson and Smith's (1971) finding in the lobster, discs were not found in histological sections several millimeters long of cardiac fibers from *Cancer magister*, suggesting that such discs are possibly absent or at least occur considerably less frequently than expected from vertebrate cardiac muscle. The presence of cytoplasmic bridges between adjacent cells is not entirely surprising for crustacean muscle, where it has long been assumed that larger muscle fibers are formed by the fusion of several smaller ones (Hoyle and Smyth, 1963). The separation between individual cardiac fibers has not been described previously. Note that all morphological and ultrastructural observations are based entirely on observations of the relatively small anterior–posterior oriented groups of myocytes, from which all experimental fibers were dissected. The results are therefore appropriate for interpreting mechanical data, but any other inferences drawn from the observations should be considered in the light of this limitation.

General passive mechanical behavior of cardiac muscle fibres

Are the passive mechanical properties of single cardiac fibers described in this paper consistent with previously reported results? A comparison with skeletal muscle fibers (Meyhöfer and Daniel, 1990) provides a partial answer to this question. Briefly, the magnitude and general trends of moduli are quite similar to those described previously for shrimp extensor fibers. Moduli range from 0.01 to 1MPa with changes in sarcomere length and strain rate and, in the physiological range, the relative energy dissipation reaches values of 0.5 and above (Meyhöfer and Daniel, 1990).

Direct comparison between my measurements and existing data is somewhat difficult because dynamic mechanical measurements on passive cardiac muscle are rare, and the few published data often do not examine the physiological range of sarcomere lengths and strain rates or consider different physiological states (rigor or active) of the muscle. There are also many observations on static mechanical properties that indicate a large variability in the passive mechanical properties between cardiac fibers of different

animals and different preparations (Fish *et al.* 1984; Fabiato and Fabiato, 1978; Tarr *et al.* 1979; Winegard, 1974). Moreover, most studies assume that only the elastic component of the passive behavior is important in determining forces that resist the elongation of muscle fibers. Data do not support this assumption and such static mechanical tests will always lead to underestimates of the total passive stiffness by as much as an order of magnitude. For example, Helber's (1980) measurements of the stiffness of relaxed frog muscle fibers show a 1Hz dynamic stiffness that is about five times larger than the static modulus at the same sarcomere length. This observation holds for the entire sarcomere length range from 2.1 to 3.0 μm. Similarly, Brady (1984) reports complex moduli for rat single fiber stiffness between 0.1 and 1MPa, whereas complex moduli calculated from the passive stiffness measurements of Fabiato and Fabiato (1978) are about an order of magnitude lower.

Nonetheless, some basic features of my observations can be confirmed by results from vertebrate dynamic experiments. For example, Pinto and Fung (1973) measured the stress relaxation and the elastic as well as the frequency response functions of rabbit passive papillary muscle. Their results agree with my findings of viscoelastic behavior of *Cancer magister* single cardiac fibers. They also found a strong nonlinear dependence of total stiffness on length and a weak dependence on strain rate (frequency). For the reference length of their muscles, they report a complex modulus of about 0.01MPa, a measure that is consistent with those measured here. Unfortunately, Pinto and Fung (1973) reported no sarcomere lengths and each of their experimental results is based on a single preparation. Total stiffness measurements of single rat cardiac myocytes (15kPa, 5Hz, 1.9 μm) (Ross and Brady, 1989; Brady and Farnsworth, 1986) agree well with my overall stiffness measurements from *Cancer magister*. Thus, at least to an order of magnitude, my estimates of cell stiffness are consistent with previous findings. Unlike past results, however, I measure a much larger range of independent variables.

Use of mechanical response surfaces and choice of models

The mechanical data presented here characterize the dynamic mechanical behavior not only in the relatively narrow physiological range of sarcomere lengths and strain rates, but also well beyond this range, describing a three-dimensional mechanical response surface for passive cardiac fibers. The relatively simple descriptive models describe the mean magnitude and gradient of the mechanical response as a function of sarcomere length and strain rate, permit statistical comparisons between different fiber types or treatments (E. Meyhöfer, in preparation) and provide algebraic expressions for direct comparison with other cells as well as for direct calculations of work requirements for cell deformations.

The selection of the specified functions reflects relationships that are either expected from the response of a simple viscoelastic body (Fung, 1981) or based on experimental observations. The total stiffness for single cardiac fibers increases approximately exponentially with sarcomere length. Such a relationship is indirectly supported by many static stiffness measurements on vertebrate cardiac fibers (for example, Fish *et al.* 1984; Fabiato and Fabiato, 1978) as well as by numerous studies on skeletal fibers (Gordon,

1989). However, the increase in dynamic stiffness with sarcomere length for the multiple-fiber cardiac preparation (E. Meyhöfer, in preparation) is better modelled by a linear relationship. To be able to compare different preparations statistically, it is necessary to fit all data sets to the same model. I therefore chose a power function, which provides a good fit for both the linear and the exponential relationships. The increase in the total dynamic stiffness with increasing strain rate is described by an inverse exponential multiplier. This form was suggested by the behavior of a standard linear model (Fung, 1981).

The dependence of the relative energy dissipation on strain rate is entirely based on Fung's (1981) standard viscoelastic model calculations. To account for the decrease in the relative energy dissipation as a function of sarcomere length, two terms increasing the value of the denominator of equation 15 with increasing sarcomere length were included. This choice was completely empirical, but proved very effective in that it was both simple and successful. One of these terms consists of the fitted multiple of the sarcomere length–strain rate product. This term allows the response surface to flex such that the apparent maximum of the relative energy dissipation could shift to lower strain rates with increasing sarcomere length. However, for none of my data sets was this possible pattern statistically verified by using the above model (equation 15), probably because the variability is large relative to this trend.

The models provide a surprisingly good description of the data. As outlined in the results section, the fitted surfaces are statistically highly significant. The addition of further variables to the models does not significantly reduce the residual sum of squares, indicating that the remaining variance is probably due to interfiber variability and not to an inadequate model. Note that the mechanical behavior of cardiac fibers predicted from these models for sarcomere lengths and strain rates outside the measured range is likely to be inaccurate. This limitation is especially severe if a steep gradient is located close to the margin of the observed data, as is the case for the possible maximum in the relative energy dissipation (see Results section).

Viscoelastic responses in the physiological parameter space: a basis for dynamic stability?

Given that the viscous component of the mechanical behavior is large in the middle of the physiological range of strains and strain rates, one must ask how significant such values are to the overall energetics of the heart. Using the data presented in this paper, I examine whether the passive energy dissipation in the cardiac fibers is large relative to the useful work done by these fibers.

The total useful work done by the heart during each beat is estimated from the pressure–volume work using the relationship:

$$W = \Delta P \Delta V, \tag{22}$$

where W is the pressure–volume work, ΔP is the systolic transmural pressure difference and ΔV is the stroke volume. Equation 22 is an approximation of the integrated time-dependent pressure–volume product, and provides satisfactory estimates of the pressure volume work (Schmidt and Thews, 1983). In addition, I neglect any work done in fluid accelerations, because estimates indicate that this work accounts for only approximately

1% of the pressure–volume work. Given a total volume of 2ml for the filled heart of a crab, a stroke volume of 30% of the volume of the filled heart (ΔV 0.6ml for 'normal' cardiac activity) and a cardiac pressure of 1000Pa, the pressure–volume work is estimated to be about 6×10^{-4} J heartbeat^{-1}.

The energy dissipation by the cardiac tissue is estimated from:

$$E_{\mathrm{d}} = 0.5E'\epsilon^2 V_{\mathrm{h}}, \tag{23}$$

where V_{h} represents the volume of cardiac tissue. The strain amplitude ϵ is estimated to be 0.1 under physiological conditions (see Results section). The mass of a heart from crabs of the size used in this study (range 0.6–0.8kg) is close to 2g (range 1.8–2.5g), which gives an approximate volume of 2.0×10^{-6} m^3. With a complex modulus of 45kPa and a value of 0.6 for the relative energy dissipation, a loss modulus of 23kPa is calculated from equation 11b. Hence, the energy dissipated in the cardiac fibers during the extension phase of each beat of the heart will be 2.5×10^{-4} J. If we assume that the same passive loss modulus is present during active shortening of the cardiac fibers, then the total amount of energy viscously dissipated rises to 5.0×10^{-4} J per cardiac cycle. This assumption is substantiated by Tidball's (1986) finding that a significant fraction of the viscous modulus is associated with the extracellular matrix, which is probably not affected by the active state of the fiber. Presumably, the same conclusion is also true for titin (connectin) and nebulin, which are now implicated as major sources of passive muscle stiffness (Horowits *et al.* 1986; Wang *et al.* 1991). This result suggests that cardiac fibers viscously dissipate a significant amount of the mechanically imparted energy, compared with the useful work done by the heart – nearly 80% of the pressure–volume work. Although these calculations are admittedly rough, even a several-fold change in any of the estimates will not change this basic conclusion that the viscous energy dissipation is large. I cannot, therefore, reject my viscous stability hypothesis. Instead, I propose that the high viscous damping of these fibers provides internal stability. A key question that arises here is what forms of mechanical instability can occur.

I can envisage three different forms of instability in the cardiac muscle system: (1) unstable motions of the whole heart, leading to undamped oscillations or ringing, (2) instabilities at the level of the single fiber in the form of non-uniform strain distributions along the length of a single fiber and (3) instabilities at the level of individual sarcomeres that cause disruptions in the regular striation pattern.

Instabilities of the whole heart (form 1) can be controlled by active mechanisms (innervation of the heart, spread of excitation signal), energy removal associated with the blood flow and its viscous loss or passive (viscous) damping the tissues of the heart. The relative importance of these control mechanisms is unknown, but I consider it unlikely that viscous damping in the cardiac fibers is necessary to achieve stability of the whole heart.

Stability at the single fiber level (form 2) requires some mechanism to dissipate mechanical strain energy, since active control at such a local level (for example, strain sensing and excitation feedback on the sarcomere) does not seem feasible. I believe that viscous damping of muscle is of great importance for the dynamic mechanical stability at this level of organization. For instance, in the case of shrimp muscle cells, Meyhöfer and

Daniel (1990) argued that the impulsive loading of the fibers during the escape response of the shrimp causes a deformation wave that will propagate along the length of the fiber with a velocity proportional to the square root of the elastic modulus (Timoshenko *et al.* 1974). In the absence of any viscous damping, the strain gradient associated with this propagating wave of deformation will be extremely steep and will yield large strain non-uniformities that may damage the internal structures. Cardiac fibers, however, are not impulsively loaded, which suggested (see Introduction) the possibility that viscous damping of these fibers is, for energetic reasons, undesirable and unnecessary to achieve internal stability. However, cardiac fibers are continuously loaded, and continuous input of energy into any system with mass and elasticity, but without any damping or mechanism to remove energy, can lead to unstable responses with undamped oscillations and ringing. Such instabilities can result in large internal strain non-uniformities. In contrast to the shrimp extensor system, I speculate that instability in a hypothetical cardiac muscle system without viscous damping would develop over many heart beats, not instantaneously.

The basis for such an argument follows from two key characteristics of vibrating systems with finite mass and elasticity. In the simplest case, a single mass with some attachment will, under continued input of vibrational energy, undergo displacements of infinite amplitude if *any* of that energy is near the resonant frequency of such a system (Timoshenko *et al.* 1974). Only with some finite amount of viscous damping can such a system respond in a stable manner to continued energy input. For such a case, ever greater damping leads to ever lower amplitudes of internal displacement.

A system consisting of a single mass, however, only illustrates the importance of damping. In a continuum model of a single cell, the mass and elasticity are spatially distributed. Thus, there is no single mass value and no single resonant frequency that characterize the system. Instead, waves of internal displacement travel along the cell (Schoenberg *et al.* 1974; Truong, 1974; T. Daniel and E. Meyhöfer, in preparation) at a characteristic velocity (equal to the square root of the elastic modulus divided by the density of the fiber), leading to an infinite set of resonant frequencies corresponding to the set of integer multiples of the number of waves present along the fiber (Farlow, 1982). Under such conditions, any continued input of energy at any one of the resonant frequencies will lead to infinite amplitudes of internal strain. With viscous damping, the steady-state amplitude will be constrained.

Although the steady-state characteristics can be clearly defined (Farlow, 1982), the transient response to vibrational motion of such a viscoelastic system is more problematic. Both the approach to steady state and the magnitude of the steady-state strain distribution are determined by the relative amount of viscous energy dissipation. Larger damping leads both to a slower rate of approach to the steady state and to a lower magnitude of internal strain at the final steady state. Thus, a passive cardiac fiber exposed to cyclic loading will develop internal strain uniformities that will build up over time. In the absence of any viscous damping, those non-uniformities will rise to infinite values as long as some component of the driving frequency is at any one of the resonant frequencies.

Horowits and Podolsky (1988) addressed an important component of the stability

problem at the level of the single sarcomere (form 3, see above): the positional stability of the thick filament in the sarcomere. Based on previous work on the structure and function of the proteins titin and nebulin (Maruyama *et al.* 1984, 1985; Wang, 1985; Gassner, 1986; Horowits *et al.* 1986; Higuchi and Umazume, 1985), they argued that the position of the myosin filament is stabilized by these large elastic proteins, which connect the myosin filament to each Z-disk. Perturbations of myosin from its center position would strain that elastic link. Thus, myosin movement causes a (passive) resting force that opposes any further myosin movement. Clearly, this mechanism depends quantitatively on the active and passive length–stiffness relationship, the sarcomere length and the initial myosin perturbation. Horowits and Podolsky (1988) formulated a 'dynamic' model that related these variables to thick filament displacement and displacement velocity. Assuming that titin is completely elastic and accounts for all of the observed resting tension, and using standard force–velocity and force–length relationships and the usual sarcomere structure, they found (1) that above 2.8 μm, the thick filament position was stable, even during very long contractions, although it was unstable under the same conditions (contraction slower than 80s) in the absence of titin, and (2) that during passive stretching, some force to recenter the myosin filament would be present if the cell was extended beyond 2.6 μm. Their first conclusion is substantiated by electron microscopical evidence (Horowits and Podolsky, 1987), but the long contraction time required for asymmetries to develop are physiologically not relevant and they concluded, therefore, that the primary physiological role of the titin filament may be to recenter the myosin filament during passive stretching and thus to prevent the slow accumulation of asymmetries in the sarcomere striation pattern over several contraction cycles.

The elastic stability hypothesis of Horowits and Podolsky provides an interesting alternative to my viscous stability hypothesis. However, I believe several aspects of their model need to be addressed. (1) Physiological strains in muscle fibers are typically only 10–20%; thus, for the fibers used, which have a resting length of 2.2 μm, the proposed mechanism might not act over the relevant range of sarcomere length but might only provide 'protection' against such instability at extreme sarcomere strains. (2) The model assumes that all of the resting stiffness of psoas fibers is produced by titin. In the next section, I discuss some of the lines of evidence supporting the idea of additional sources of stiffness in passive fibers. Any reduction of the stiffness due to titin reduces quantitatively the ability of the proposed mechanism to provide mechanical stability (3) Titin, if it accounts for most of the passive behavior in the relevant range of sarcomere lengths, as argued by Horowits *et al.* (1986), is viscoelastic, as shown by the stress relaxation in their published tension records. (4) The proposed static model does not consider dynamic perturbations in fiber length and their consequences. The response of the model to dynamic strain (sarcomere length) non-uniformities and to steep strain gradients is unclear. Any mechanism that yields stability based on an increased passive elasticity of the muscular system is potentially undesirable, because increased passive elastic (or viscoelastic) resistance reduces contraction velocity and, hence, power output (Mirsky and Krayenbuchl, 1981; Pollack, 1970; Natarajan *et al.* 1979). Thus, the 'elastic stability mechanism' might well be energetically more expensive than viscous damping.

Elastic energy storage in the physiological parameter space: is the crustacean heart a mechanical resonator?

In a manner similar to the viscous energy losses, we can estimate the elastic energy stored during passive extension of the heart using the following relationship:

$$E_s = 0.5E'\epsilon^2 V_h . \tag{24}$$

Using the above estimates and equation 11a, the elastically stored energy amounts to about 3.8×10^{-4} J. This energy can be returned during the contractile phase. Nevertheless, the structure(s) extending the heart during the refilling phase of the cardiac cycle has to provide the energy to overcome the sum of elastic and viscous resistances, which amount to 3.8×10^{-4} and 2.5×10^{-4} J, respectively, giving a value that is larger than the pressure–volume work done by the heart. This estimate does not include any pressure–volume work necessary to fill the heart.

These calculations raise an important question: which structure or physiological function is responsible for extending and filling the heart? Hearts of crustaceans, and arthropods in general, are suspended by a number of elastic ligaments that connect the heart to adjacent apodemes of the exoskeleton (Krijgsman, 1952). It seems plausible that the heart of *Cancer magister* operates as a resonating system, in which passive strain energy is continuously exchanged between the passive component of the cardiac fibers and the ligaments. My calculations indicate that the ligaments must elastically store and then return at least 6.3×10^{-4} J in each cardiac cycle, whereas the muscle fibers store and return 3.8×10^{-4} J. A comparison with the useful work done (pressure–volume work, 6.0×10^{-4} J) shows that the elastic energy stored (energy savings) represents a significant component of the energy budget for a heart beat. Assuming that the fluid-dynamic energy losses associated with the pumping action of the heart are about half the pressure–volume work (an extremely pessimistic estimate) and purely elastic behavior in the ligaments, then the total work (pressure–volume work, stretching of the ligaments, energy dissipation in the fluid and the cardiac fibers) done by the heart in a single beat is approximately 1.8mJ; about 3.8×10^{-4} J of this energy was elastically stored and returned. Although such calculations are only approximations, they indicate an energy saving of about 20%, which suggests the possibility that the heart pump in this system behaves as a resonating system.

Circumstantial evidence for the resonance behavior comes from pressure recordings. When a heart starts to beat again after a rest period (Fig. 3) its pressure amplitude rises over several beat to a new steady state. Such behavior is to be expected from a resonant system. There is, however, no direct evidence that the system has a resonance at 1Hz. In fact, it is possible that the slow increase in cardiac pressure after a rest period is due to a phenomenon similar to the *Treppe* observed for vertebrate cardiac muscle (Huntsman and Feigl, 1989). Nevertheless, I find it very interesting that the heart of all animals always beats at exactly one frequency (very close to 1Hz) and that it stops intermittently to adjust to lowered circulatory demands (Fig. 3B) rather than following the vertebrate strategy of regulating the beat frequency.

In this discussion, I have presented results supporting two apparently conflicting

hypotheses: that the heart of *Cancer magister* dissipates energy to attain dynamic mechanical stability; and that it simultaneously stores and returns elastic strain energy in a resonating system to conserve energy. I believe there is no conflict. The need for viscous energy dissipation at the level of the single fiber for mechanical strain stability does not preclude efficient and energy-saving strategies from the cardiac system.

What is the structural basis for the mechanical behavior?

The significant linear relationship between the ECM volume fraction and the total stiffness suggests that the ECM is an important determinant of the passive mechanical behavior of the heart. My measurements do not, however, explain the extent to which the ECM determines the passive mechanics. Different structural components and mechanism have been implicated as the source of passive stiffness. Unfortunately, only very few studies have relied on dynamic mechanical measurements.

Several different structures and physiological functions have been implicated in passive dynamic stiffness: (1) the ECM (Tidball, 1986; Winegard, 1974); (2) the extracellular skeletal framework with its large collagen and elastin fibers, large intercellular struts (bundles of collagen fibrils) and microthreads and fibrils (Robinson *et al.* 1983, 1985; Borg *et al.* 1981*a*,*b*; Orenstein *et al.* 1980; Tarr *et al.* 1979); (3) titin (connectin, projectin), nebulin and possibly other large structural proteins associated with myofibrillar structures (Granzier and Wang, 1993; Horowits *et al.* 1986; Hu *et al.* 1990; Maruyama, 1986; Maruyama *et al.* 1977*a*,*b*,*c*; Wang *et al.* 1991); (4) viscous forces associated with the sliding motion of filaments in the sarcomere (Ernst, 1977); (5) weak actin–myosin interactions (Brenner *et al.* 1982, 1984; Granzier and Wang, 1993); and (6) short-range elasticity (Hill, 1968).

A detailed comparison of these various mechanisms is beyond the scope of this discussion, but some exclusions can be made. For example, the short-range elasticity of muscle and the weak binding of acto-myosin in relaxed muscle are unlikely to contribute significantly to the (total) stiffness of muscle; the elastic limit of the short-range elasticity (Hill, 1968) is so small that physiological length changes (and even small sinusoidal length perturbations, Helber, 1980) exceed it by more than 100-fold. Weak acto-myosin interactions in vertebrate skeletal muscle fibers lead to measurable changes in fiber stiffness only in low ionic strength solutions and when rapid stretches are applied (Brenner *et al.* 1982, 1984), suggesting that such crossbridges do not contribute to passive fiber stiffness under physiological conditions. Granzier and Wang (1993) recently reported that fibers from the indirect flight muscles of the waterbug *Lethocerus* also exhibit weak acto-myosin interaction at physiological ionic strength, but their stiffness measurements were carried out using very rapid length changes (2.2kHz sinusoids). For cardiac fibers, such deformation rates are well above the *in vivo* strain rates and are physiologically not relevant. Furthermore, if the dynamic mechanical properties measured in the present study were based on weak crossbridge interactions, we would expect the stiffness to decline linearly with increasing sarcomere length. However, both the elastic and viscous moduli increase steeply with sarcomere length.

The viscous resistance due to the relative sliding of thick and thin filaments can be calculated directly by adopting the following simplified geometry for muscle: the thick

filament is a cylinder with radius r_i that is displaced along its axis in a larger cylinder of radius r_o formed by the six actin filaments surrounding the thick filament. The viscous force on a single myosin filament moving with velocity v is given by:

$$F_v = 2\pi\eta l v/[\ln(r_i/r_o)], \tag{25}$$

where η denotes the viscosity of the fluid in the gap between the two cylinders (Huxley, 1980; notice the misprint in the formula on page 66). This formula is the solution of a simplified version of the Navier–Stokes equation, from which inertial terms have been dropped and the fluid density and viscosity are to be assumed constant. With the appropriate boundary conditions, the velocity can be found as a function of radius r (for an outline of this approach, see Bird *et al.* 1960), and the viscous shear force on a single filament (F_v) can be determined from the spatial velocity gradient. For the cardiac muscle of *Cancer magister*, I assume the following values. The radius of the thick filaments, measured from electron micrographs (Fig. 2B), is approximately 8nm. I estimate the radius of the cylinder formed by the actin filaments to be 25nm. The overlap of actin and myosin at 4.0 μm (lower end of physiological range) is about 1.5 μm and the viscosity of the fluid in the interfilament space is about 2.0×10^{-3} Pas (see discussion in Huxley, 1980). I estimate the relative sliding velocity of the filaments for my experimental perturbations from a root-mean-square value of the strain rate. The sliding velocity equivalent to the physiological strain rate of 0.6rad s^{-1} is 6.3×10^{-7} m s^{-1}. Thus, the viscous force on a single myosin filament is approximately 1.0×10^{-14} N. With about 3×10^{14} myosin filaments per square meter (myofibrillar volume fraction equals 0.5) and a typical strain of about 1% in the experiments reported here, the resultant viscous modulus is approximately 300Pa. This calculation is obviously very rough, but it indicates that the viscous modulus expected from the relative sliding of the filaments is significantly smaller than the measured value (less than 10% of my lowest value for E''). This result is in agreement with Huxley's (1980) calculation that the viscous stress due to filament sliding at the fastest shortening velocity represents a negligible fraction of the maximum isometric stress. In addition, on the basis of the linear dependence of the viscous force F_v (equation 23) on the filament overlap (l), I expect the force to decline linearly with increasing sarcomere length. However, exactly the opposite observation is true (e.g. Fig. 4), further supporting the idea that the viscous moduli observed here are not due to interfilament viscosity, but are based on a different mechanism.

This leaves two different structural components to be considered: the large myofibrillar proteins titin (connectin, projectin) and nebulin, and the extracellular structural matrix, including the ECM (basement membrane). The work in this paper provides sound evidence that the ECM in cardiac fibers of *Cancer magister* plays an important role in the passive mechanical behavior at longer sarcomere length (above 5.0 μm), where the ultrastructural data presented here were collected. The strong linear correlation between the 'amount' of ECM and the mechanics of the fiber suggests that a large component of the mechanical behavior at this sarcomere length is determined by the ECM. Unfortunately, this study does not provide direct observations at shorter sarcomere lengths, and it is difficult, if not impossible, to extrapolate these results to shorter sarcomere lengths.

Further support for the role of the ECM in the passive behavior comes from the dynamic mechanical experiments of Tidball (1986), who showed that the ECM is a major contributor to the total dynamic stiffness. Upon enzymatic digestion of the ECM, the total stiffness declined about threefold, whereas the viscous modulus declined about tenfold. Tidball's data also help us to understand the large variability in the moduli reported here.

The potential role of connectin (titin), nebulin and related proteins has been stressed. The experiments of Horowits *et al.* (1986, also see above discussion) provide strong evidence for a function for these macromolecules in the passive mechanical behavior. However, I am not convinced by the claim (Horowits *et al.* 1986; Murayama, 1986; Magid and Law, 1985) that these structural proteins account for almost all of the passive stiffness. For example, Magid and Law (1985) argue that, in frog skeletal muscle at fibres lengths below 3.8 μm (resting length is about 2.2 μm), the resting tension resides in the myofibrillar component, not in the connective tissue. However, their own data show that the modulus of mechanically skinned fibers (ECM stripped off) is only about half that of intact single fibers.

On the evidence currently available, I consider it more probable that both the extracellular matrix with its associated connective tissue and the myofibrillar proteins are important determinants of the passive mechanics of single fibers. The stability hypotheses proposed here and by Horowits and Podolsky (1988) provide a possible explanation for the need for both components: myofibrillar proteins, such as connectin, provide positional stability for myosin filaments at longer sarcomere lengths, whereas the viscous damping endows fibers with a mechanism providing stability against length non-uniformities.

This work was supported by a grant from the Whitaker Foundation to T. Daniel. I wish to thank Dr T. Daniel for his help throughout the duration of this project. Drs T. Daniel J. Howard, A. M. Gordon and an anonymous referee read versions of the manuscript and provided many helpful suggestions. The author is currently a fellow of the Washington Affiliate of the American Heart Foundation.

References

ANDERSON, M. E. AND SMITH, D. S. (1971). Electrophysiological and structural studies on the heart muscle of the lobster *Homarus americanus. Tissue & Cell* **3**, 191–205.

ATWOOD, H. L. (1973). An attempt to account for the diversity of crustacean muscles. *Am. Zool.* **13**, 357–378.

BENDAT, J. S. AND PIERSOL, A. G. (1980). *Engineering Applications of Correlation and Spectral Analysis*. New York: John Wiley.

BENDAT, J. S. AND PIERSOL, A. G.(1986). *Random Data.* New York: John Wiley.

BEVINGTON, P. R. (1969). *Data Reduction and Error Analysis for the Physical Sciences*. New York: McGraw-Hill.

BIRD, R. E., STEWARD, W. E. AND LIGHTFOOT, E. N. (1960). *Transport Phenomena.* New York: John Wiley.

BORG, T. K. AND CAULFIELD, J. B. (1981*a*). The collagen matrix of the heart. *Fedn Proc. Fedn Am. Socs exp. Biol.* **40**, 2037–2041.

BORG, T. K., RANSON, W. F., MOSLEHY, F. A. AND CAULFIELD, J. B. (1981*b*). Structural basis of ventricular stiffness. *Lab. Invest.* **44**, 49–54.

BRADY, A. J.(1984). Passive stiffness of rat cardiac myocytes. *J. Biomech. Eng.* **106**, 25–30.

BRADY, A. J. AND FARNSWORTH, S. P. (1986). Cardiac myocyte stiffness following extraction with detergent and high salt solutions. *Am. J. Physiol.* **250**, H932–H943.

BRENNER, B., SCHOENBERG, M., CHALOVICH, J. M., GREENE, L. E. AND EISENBERG, E. (1982). Evidence for cross-bridge attachment in relaxed muscle at low ionic strength. *Proc. natn. Acad. Sci. U.S.A.* **79**, 7288–7291.

BRENNER, B., YU, L. C. AND PODOLSKY, R.(1984). X-ray diffraction evidence for cross-bridge formation in relaxed muscle fibers at various ionic strengths. *Biophys. J.* **46**, 299–306.

BROZOVICH, F. V., YATES, L. D. AND GORDON, A. M.(1988). Muscle force and stiffness during activation and relaxation. *J. gen. Physiol.* **91**, 399–420.

BUCHTHAL, F. AND ROSENFALCK, P.(1957). Elastic properties of striated muscle. In *Tissue Elasticity* (ed. J. W. Remington), pp. 73–97. Baltimore: Waverly Press.

CHRISTENSEN, R. M.(1982). *Theory of Viscoelasticity.* New York: Academic Press.

DRAPER, N. R. AND SMITH, H.(1981). *Applied Regression Analysis.* New York: John Wiley.

ERNST, E.(1977). Sliding friction contra sliding hypothesis. *Acta biochim. biophys.* **12**, 83–85.

FABIATO, A. AND FABIATO, F.(1978). Myofilament-generated tension oscillations during partial calcium activation and dependence of sarcomere length–tension relation of skinned cardiac cells. *J. gen. Physiol.* **72**, 667–699.

FABIATO, A. AND FABIATO, F. (1979). Calculator programs for computing the composition of the solutions containing multiple metals and ligands used for experiments in skinned muscle cells. *J. Physiol., Paris* **75**, 463–505.

FARLOW, S. J. (1982). *Partial Differential Equations for Scientists and Engineers.* New York: John Wiley.

FERRY, J. D.(1980). *Viscoelastic Properties of Polymers.* New York: John Wiley.

FISH, D., ORENSTEIN, J. AND BLOOM, S. (1984). Passive stiffness of isolated cardiac and skeletal myocytes in the hamster. *Circulation Res.* **54**, 267–276.

FRANZINI-ARMSTRONG, C., EASTWOOD, A. B. AND PEACHEY, L. D.(1986). Shape and disposition of clefts and sarcoplasmic reticulum in long and short sarcomere fibers of crab and crayfish. *Cell Tissue Res.* **244**, 9–19.

FUNG, Y. C. (1981). *Biomechanics: Mechanical Properties of Living Tissues*. New York: Springer-Verlag.

FUNG, Y. C.(1984). Structure and stress–strain relationships of soft tissues. *Am. Zool.* **24**, 13–22.

GASSNER, D. (1986). Myofibrillar interaction of blot immuno-affinity purified antibodies against native titin as studied by direct immunofluorescence and immunogold staining. *Eur. J. Cell Biol.* **40**, 176–184.

GORDON, A. M. (1989). Molecular basis of contraction. In *Textbook of Physiology* (ed. H. D. Patton, A. F. Fuchs, B. Hille, A. M. Scher and R. A. Steiner), pp. 171–195. Philadelphia: W. B. Saunders.

GRANZIER, H. L. M. AND WANG, K. (1993). Interplay between passive tension and strong and weak cross-bridges in insect indirect flight muscles. *J. gen. Physiol.* **101**, 235–270.

HELBER, R. (1980). Elastic and inelastic behavior of resting frog muscle fibers. *Pflügers Arch.* **387**, 261–268.

HIGUCHI, H. AND UMAZUME, Y. (1985). Localization of the parallel elastic components in frog skinned muscle fibers studied by the dissociation of A- and I-bands. *Biophys. J.* **48**, 137–147.

HILL, D. K. (1968). Tension due to interaction between sliding filaments in resting striated muscle. The effect of stimulation. *J. Physiol., Lond.* **199**, 637–684.

HOROWITS, R., KEMPNER, E. S., BISHER, M. E. AND PODOLSKY, R. J.(1986). A physiological role for titin and nebulin in skeletal muscle. *Nature* **323**, 160–164.

HOROWITS, R. AND PODOLSKY, R. J. (1987). The positional stability of thick filaments in activated skeletal muscle depends on sarcomere length: evidence for the role of titin filaments. *J. Cell Biol.* **105**, 2217–2223.

HOROWITS, R. AND PODOLSKY, R. J.(1988). Thick filaments movement and isometric tension in activated skeletal muscle. *Biophys. J.* **54**, 165–171.

HOYLE, G.(1983). *Muscles and their Neural Control.* New York: John Wiley.

HOYLE, G. AND SMYTH, T. (1963). Neuromuscular physiology of giant muscle fibers of a barnacle, *Balanus nubilus* Darwin. *Comp. Biochem. Physiol.* **10**, 291–314.

HU, D. H., MATSUNO, A., TERAKADO, K., KIMURA, S. AND MARUYAMA, K. (1990). Projection is an invertebrate connectin (titin): isolation from crayfish claw muscle and localization in crayfish claw and insect flight muscle. *J. Muscle Res. Cell Motil.* **11**, 497–511.

HUNTSMAN, L. L. AND FEIGL, E. O. (1989). Cardiac mechanics. In *Textbook of Physiology* (ed. H. D. Patton, A. F. Fuchs, B. Hille, A. M. Scher and R. A. Steiner), pp. 820–833. Philadelphia: W. B. Saunders.

HUXLEY, A. F. (1980). *Reflections on Muscle*. Princeton: Princeton University Press.

KRIJGSMAN, B. P. (1952). Contractile and pacemaker mechanisms of the hearts of arthropods. *Biol. Rev.* **27**, 320–341.

MAGID, A. AND LAW, D. J. (1985). Myofibrils bear most of the resting tension in frog skeletal muscle. *Science* **230**, 1280–1282.

MARUYAMA, K.(1986). Connectin, an elastic filamentous protein of striated muscle. *Int. Rev. Cytol.* **104**, 81–114.

MARUYAMA, K., KIMURA, S., KURODA, M. AND HANDA, S. (1977*a*). Connection, an elastic protein of muscle. Its abundance in cardiac myofibrils. *J. Biochem., Tokyo* **82**, 347–350.

MARUYAMA, K., MATSUBARA, S., NATORI, R., NONOMURA, Y., KIMURA, S., OHASHI, K., MURAKAMI, F., HANDA, S. AND EGUCHI, G. (1977*b*). Connectin, an elastic protein of muscle. Characterization and function. *J. Biochem., Tokyo* **82**, 317–337.

MARUYAMA, K., MURAKAMI, F. AND OHASHI, K. (1977*c*). Connectin, an elastic protein of muscle. Comparative biochemistry. *J. Biochem., Tokyo* **82**, 339–345.

MARUYAMA, K., SAWADA, H., KIMURA, S., OHASHI, K., HIGUCHI, H. AND UMAZUME, Y. (1984). Connectin filaments in stretched skinned fibers of frog skeletal muscle. *J. Cell Biol.* **99**, 1391–1397.

MARUYAMA, K., YOSHIOKA, T., HIGUCHI, H., OHASHI, K., KIMURA, S. AND NATORI, R. (1985). Connectin filaments link thick filaments and Z-line in frog skeletal muscle as revealed by immunoelectron microscopy. *J. Cell Biol.* **101**, 2167–2172.

MEYHÖFER, E. AND DANIEL, T. L. (1990). Dynamic mechanical properties of extensor muscle cells of the shrimp *Pandalus danae*: cell design for escape locomotion. *J. exp. Biol.* **151**, 435–452.

MIRSKY, I. AND KRAYENBUCHL, H. P. (1981). The role of wall stress in the assessment of ventricular function. *Herz* **6**, 288–299.

NATARAJAN, G., BOVE, A. A., COULSON, R. L., CAREY, R. A. AND SPANN, J. F.(1979). Increased passive stiffness of short-term pressure-overload hypertrophied myocardium in cat. *Am J. Physiol.* **237**, H676–680.

ORENSTEIN, J., HOGAN, D. AND BLOOM, S. (1980). Surface cables of cardiac myocytes. *J. molec. cell. Cardiol.* **12**, 771–780.

PINTO, J. G. AND FUNG, Y. C. (1973). Mechanical properties of the heart muscle in the passive state. *J. Biomechanics* **6**, 597–616.

POLLACK, G. H. (1970). Maximum velocity as an index of contractility in cardiac muscle: critical evaluation. *Circulation Res.* **26**, 111–127.

PRESS, W. H., FLANNERY, B. P., TEUKOLSKY, S. A. AND VETTERLING, W. T.(1989). *Numerical Recipes in Pascal*. Cambridge: Cambridge University Press.

PRIESTLEY, M. B.(1981). *Spectral Analysis and Time Series*. London: Academic Press.

RAMSEY, R. W. AND STREET, S. F. (1940). The isometric length–tension diagram of isolated skeletal muscle fibers of the frog. *J. cell. comp. Physiol.* **15**, 11–34.

ROBINSON, T. F., COHEN-GOULD, L. AND FACTOR, S. M.(1983). Skeletal framework of mammalian heart muscle. *Lab. Invest.* **49**, 482–498.

ROBINSON, T. F., COHEN-GOULD, L., REMILY, R. M., CAPASSO, J. M. AND FACTOR, S. M. (1985). Extracellular structures in heart muscle. In *Advances in Myocardiology*, vol. 5 (ed. P. Harris and P. A. Poole-Wilson), pp. 243–255. New York: Plemum Press.

ROSS, K. P. AND BRADY, A. J. (1989). Stiffness and shortening changes in myofilament-extracted rat cardiac myocytes. *Am. J. Physiol.* **256**, H539–H551.

SANGER, J. W.(1979). Cardiac fine structure in selected arthropods and molluscs. *Am. Zool.* **19**, 9–27.

SCHMIDT, R. F. AND THEWS, G.(1983). *Human Physiology*. Berlin: Springer Verlag.

SCHOENBERG, M., WELLS, J. B. AND PODOLSKY, R. J. (1974). Muscle compliance and the longitudinal transmission of mechanical impulses. *J. gen. Physiol.* **64**, 623–642.

SEBER, G. A. F. AND WILD, C. J.(1989). *Nonlinear Regression*. New York: John Wiley.

SMITH, D. S. AND ANDERSON, M. E.(1972). The disposition of membrane systems in cardiac muscle of a lobster, *Homarus americanus*. *Tissue & Cell* **4**, 629–645.

SONNENBLICK, E. H. AND SKELTON, C. L. (1974). Reconsideration of the ultrastructural basis of the contractile process in the heart and skeletal muscle. *Circulation Res.* **35**, 517–526.

SPERELAKIS, N. (1970). Ultrastructure of the neurogenic heart of *Limulus polyphemus*. *Z. Zellforsch. mikrosk. Anat.* **116**, 443–463.

SQUIRE, J. (1981). *The Structural Basis of Muscular Contraction.* New York: Plenum Press.

STROBECK, J. E. AND SONNENBLICK, E. H. (1986). Myocardial contractile properties and ventricular performance. In *The Heart and Cardiovascular System* (ed. H. A. Fozzard, E. Haber, R. B. Jennings, A. M. Katz and H. E. Morgan), pp. 31–49. New York: Raven Press.

TARR, M., TRANK, J. W., LEIFFER, P. AND SHEPPARD, N. (1979). Sarcomere length–resting tension relation in single frog atrial cardiac cells. *Circulation Res.* **45**, 554–559.

TIDBALL, J. G. (1986). Energy stored and dissipated in skeletal muscle basements membranes during sinusoidal oscillations. *Biophys. J.* **50**, 1127–1138.

TIMOSHENKO, S., YOUNG, D. H. AND WEAVER, W. (1974). *Vibration Problems in Engineering*. New York: John Wiley.

TRUONG, X. T.(1974). Viscoelastic wave propagation and rheologic properties of skeletal muscle. *Am. J. Physiol.* **226**, 256–264.

WAINWRIGHT, S. A., BIGGS, W. D., CURREY, J. D. AND GOSLINE, J. M. (1976). *Mechanical Design in Organisms*. London: Edward-Arnold.

WANG, K. (1985). Sarcomere-associated cytoskeletal lattices in striated muscle. *Cell Muscle Motil*. **6**, 315–369.

WANG, K., MCCARTER, R., WRIGHT, J., BEVERLY, J. AND RAMIREZ-MITCHELL, R. (1991). Regulation of skeletal muscle stiffness and elasticity by titin isoforms: a test of the segmental length extension model of resting tension. *Proc. natn. Acad. Sci. U.S.A.* **88**, 7101–7105.

WINEGARD, S.(1974). Resting sarcomere length–tension relation in living frog heart. *J. gen. Physiol.* **64**, 343–355.

ZAR, J. H. (1984). *Biostatistical Analysis.* Englewood Cliffs: Prentice-Hall.